Environmental Processes (2026) 13:25
https://doi.org/10.1007/s40710-026-00832-3

RESEARCH

Menthol-Based Hydrophobic Deep Eutectic Solvents: Tunable Polarity, Interfacial Properties, Antimicrobial Activity, and Liquid–Liquid Microextraction of Organic Pollutants

Victoria Vorobyova[1] · Georgii Vasyliev[1] · Oleksiy Myronyuk[1] · Inna Trus[1] · Margarita Skiba[2]

Received: 25 January 2026 / Accepted: 23 April 2026

Abstract

Hydrophobic deep eutectic solvents (HDES) are emerging as sustainable and tunable alternatives to conventional organic solvents due to their low toxicity, environmental compatibility, and adjustable physicochemical properties. This study investigated the influence of hydrogen-bond donor type on the structure, surface properties, antibacterial activity, and extraction performance of menthol-based HDES, assessing their potential for environmental remediation. Five HDES were synthesized using levulinic acid, acetic acid, lactic acid, oleic acid, and linalool as hydrogen-bond donors and characterized by nuclear magnetic resonance and infrared spectroscopy. Quantum-chemical calculations predicted donor reactivity and hydrogen-bonding interactions. Surface properties, including interfacial tension, contact angles, drop volume, and surface energy components, were measured, and polarity was determined using a solvatochromic probe. Antibacterial activity was tested against Gram-positive and Gram-negative bacteria and Candida species. Extraction efficiency of methylene blue and diclofenac from aqueous solutions was evaluated to assess pollutant removal. The HDES exhibited low interfacial tension and dispersive-dominated surface energy, confirming their hydrophobic nature. Polarity was tunable according to hydrogen-bond donor type, with menthol–linalool HDES showing the strongest antibacterial activity. Extraction efficiencies ranged from 65 to 84% for methylene blue and 7 to 52% for diclofenac, highlighting the importance of donor selection, polarity, and viscosity. Greenness evaluation using BAGI and ComplexGAPI tools confirmed superior environmental performance of the synthesized HDES. Menthol-based HDES thus provide multifunctional properties, combining tunable polarity, bioactivity, and efficient pollutant extraction. They represent a promising class of environmentally friendly solvents for water purification, analytical applications, and sustainable chemical processes.

Highlights

- Menthol-based HDES were synthesized using five hydrogen bond donors.
- The HDES exhibited low interfacial tension and dispersive surface energy.
- Solvent polarity was tuned by selecting hydrogen bond donors ($E_N R \approx 52$–57 kcal/mol).
- Menthol–linalool HDES showed the strongest antibacterial activity.

Extended author information available on the last page of the article

Published online: 05 May 2026

- The HDES efficiently extracted methylene blue and diclofenac.

Keywords Menthol-based HDES · Hydrogen-bonding interactions · Molecular electrostatic potential · Surface tension · Green solvents

1 Introduction

Among the wide range of deep eutectic solvents (DES) that have been extensively studied, the majority of those synthesized until recently have been hydrophilic in nature (Abranches and Coutinho 2022; Cao and Su 2021; Zheng et al. 2025a, b; Thiamngoen et al. 2024). This intrinsic hydrophilicity has significantly limited their practical applications, particularly in the separation of aqueous samples or in lipophilic analytical processes, in the extraction of natural hydrophobic compounds from plant raw materials. To overcome this fundamental limitation, a new generation of hydrophobic deep eutectic solvents (HDES) has emerged since 2015, leading to a rapid expansion in research focused on their synthesis and applications (Cao and Su 2021; Castro et al. 2023; Plyduang et al. 2025). The development of HDES has been primarily driven by the need to extend the functional range of DES and provide "green" alternatives to conventional organic solvents. HDES are classified as fifth-generation solvents, distinguished from earlier DES types by their intrinsic water immiscibility and unique phase behavior. HDES are eutectic mixtures characterized by water immiscibility and a strong solvating ability toward both organic and inorganic compounds. They are typically formed from poorly water-soluble components. In analytical chemistry, HDES are defined as solvents capable of forming biphasic systems with aqueous media. Due to their tunable physicochemical properties, low toxicity, and environmental compatibility, HDES are increasingly regarded as promising sustainable alternatives to traditional volatile organic solvents in sample preparation and extraction techniques (Viñas-Ospino et al. 2023a, b; Sportiello et al. 2023; Pishro et al. 2025; Ribeiro et al. 2015; Bochko et al. 2025; Vorobyova et al. 2022, 2023, 2024).

Among various types of HDES, menthol-based systems represent one of the most rapidly developing families. The concept of natural HDES was introduced through combinations of DL-menthol or *L*-menthol is a naturally occurring monoterpene with extremely low water solubility with a variety of hydrogen bond donors (HBDs). Menthol acts as a hydrogen bond acceptor (HBA) and can be combined with several classes of HBDs, including long-chain organic acids, such as octanoic (OctA), decanoic (DecA), dodecanoic (DoDecA), tetradecanoic (tDecA), hexadecanoic (HexDecA), and octadecanoic (OctDecA) acids (Viñas-Ospino et al. 2023a, b; Bochko et al. 2025; Vorobyova et al. 2023), short-chain organic acids, including acetic (AceA) (Ferreira et al. 2026), pyruvic (PyrA), and lactic (LacA) acids. For instance, *L*-menthol forms a natural deep eutectic solvent with formic acid in a 1:2 molar ratio. These menthol-based HDES systems exhibit excellent hydrophobicity, tunable viscosity, and enhanced extraction performance, which makes them particularly attractive for cosmetic, pharmaceutical, and analytical applications.

Despite these advances, systematic investigations linking the molecular structure of HDES components with their physicochemical behavior and functional performance remain limited. Much of the comparative literature to date has focused on gradients within structurally similar hydrogen bond donors (e.g., varying fatty acid chain lengths) (Siddiqui and

Ali 2026; Falahudin et al. 2025; Bochko et al. 2025), but there is a notable gap in the understanding of how transitions between distinct chemical classes of donors (e.g., from carboxylic acids to terpene alcohols) affect solvent properties such as polarity, viscosity, hydrophobicity, and bioactivity (López-Flores et al. 2025; Kumar et al. 2024). This gap is especially apparent for HDES systems incorporating terpene alcohols like linalool, which possess intrinsic aroma and natural occurrence in botanicals and could offer dual functional benefits in extraction efficiency and sensory properties of extracts.

Additionally, while HDES have demonstrated promising performance in the extraction of diverse organic solutes, metal ions, and pollutants (Shahzad et al. 2026), few studies have systematically addressed the interplay between solvent composition, hydrogen-bonding interactions, and extraction outcomes under identical experimental conditions (Zheng et al. 2025a, b; Ferreira et al. 2026). The existing literature underscores the potential but also the complexity of HDES design, stressing the need for rational studies to delineate structure–property–function relationships that can guide the targeted development of HDES for analytical, pharmaceutical, and cosmetic applications.

Taken together, these observations highlight an important research gap: the lack of comprehensive, comparative studies on menthol-based HDES with different HBD types that span distinct chemical classes and their impact on physicochemical and functional properties. Addressing this gap is crucial for optimizing solvent design and fully harnessing the potential of HDES as sustainable, tunable media. This study therefore aims to perform quantum-chemical evaluation of HBD reactivity, comprehensive synthesis, and characterization of menthol-based HDES, and systematic assessment of their physicochemical performance to elucidate underlying structure – property relationships. The extraction efficiency toward model dyes was examined to evaluate the potential use of the synthesized HDES in environmental remediation.

The present study addresses the research question of how the nature of hydrogen-bond donors affects the physicochemical properties and functional performance of menthol-based HDES. Particular attention is given to understanding structure – property relationships that influence their extraction efficiency toward model pollutants in aqueous systems. The novelty of this work lies in the comprehensive investigation of HDES surface properties, antibacterial activity, and extraction performance toward dyes as model contaminants to evaluate their potential application in environmentally relevant pollutant removal processes. In addition, the menthol – linalool HDES system is investigated for the first time, providing new insights into the development of sustainable solvent systems for environmental monitoring and water purification technologies.

2 Experimental Sections

2.1 Chemicals

The chemicals used in this study, as summarized in Table 1, include DL-menthol (CAS No. 89–78–1, purity ≥ 95%) as the HBA and several HBDs, including: *DL*-lactic acid (CAS No. 50–21–5, purity > 85%), acetic acid (CAS No. 64–19–7, purity ≥ 99%), levulinic acid (CAS No. 123–76–2, purity ≥ 98%), oleic acid (CAS No. 112–80–1, purity ≥ 99%), and linalool (CAS No. 78–70–6, purity ≥ 97%). Sodium diclofenac (DIC) (≥ 99% purity) was obtained

Table 1 Chemicals used for the synthesis of the HDESs in this study

HBA	HBD	Abbreviations	Organoleptic stability
Menthol	Levulinic acid	HDES-1	Colorless liquid
	Acetic acid	HDES-2	Colorless liquid
	Lactic acid	HDES-3	Colorless liquid
	Oleic acid	HDES-4	Yellow homogenous liquid
	Linalool	HDES-5	Colorless liquid

from Sigma-Aldrich and used as received without further purification. All chemicals were used as received without further purification. Deionized water was used for all solution preparations.

2.2 Computer Simulation

The reactivity of selected organic compounds was evaluated using Hyper Chem software (Shah et al. 2025; Guidugli and Reza 2025; Cysewski et al. 2025) Molecular geometry optimization was performed by means of semi-empirical quantum mechanical calculations employing the extended PM3 method. During the optimization process, MM+ force fields (based on the MM2 model) were applied. The Hyper Chem program was further used to visualize 3D isosurfaces, total charge density, molecular orbitals and the electrostatic potential (ESP) maps of the studied molecules. Key electronic parameters that determine the potential for hydrogen bond formation between donor and acceptor sites. Formulas for calculating quantum-chemical parameters are presented in Supplementary Material (SM) Section SM1. Reactivity indices were derived from these parameters according to established theoretical formulas SM1-SM8 of SM. The correlation between molecular energy calculated via the density functional approach and chemical reactivity is discussed in references (Guidugli and Reza 2025; Cysewski et al. 2025; Chen et al. 2025; Shakourian-Fard et al. 2021; Singh et al. 2024; Zheng et al. 2025a, b; Rodríguez-Juan et al. 2021; Li et al. 2025; Vorobyova 2023).

2.3 Preparation of HDES

HDES were prepared by mixing the selected components in the predetermined molar ratio (mol/mol) (Table 1). The mixtures were subsequently heated at 50 °C under continuous magnetic stirring until a transparent and homogeneous liquid was formed. The stirring was maintained throughout the heating process to ensure complete dissolution and uniformity of the solvent. Once prepared, the HDES were cooled to room temperature and stored in airtight containers until further.

2.4 Nuclear Magnetic Resonance Spectroscopy (^{1}H and C^{13} NMR) of HDES

HDESs were dissolved in a deuterated solvent to prepare the NMR sample. Conduct the ^{1}H NMR and C^{13} experiment using an appropriate NMR spectrometer, typically operating at 300–600 MHz for proton NMR (Vorobyova et al. 2023). Each spectrum was recorded with 120 scans and 48 K data points.

2.5 FTIR Spectroscopy of HDES

To confirm the theoretically predicted interaction through the functional reactive groups of the compounds. Fourier transform spectra were experimentally obtained. Fourier transform infrared (FTIR) spectra were recorded using a PerkinElmer Spectrum. Two FTIR spectrometer with a spectral resolution of 0.5 cm^{-1} in the range of 400–4000 cm^{-1} (Vorobyova et al. 2022, 2023; Malik et al. 2022; Thiamngoen et al. 2024).

2.6 Antibacterial Activity of HDES

Test strains, including the Gram-negative bacterium Escherichia coli (*E. coli*) UKM B-906 and the Gram-positive spore-forming Bacillus subtilis (*B. subtilis*) UCM B-506T, were obtained from the Danylo Zabolotny Institute of Microbiology and Virology of the National Academy of Sciences of Ukraine (Huang et al. 2021). The antibacterial activity of the HDES was evaluated against both Gram-positive and Gram-negative bacteria using the disk diffusion method (DDT). Before testing, the bacterial inoculum was cultured in liquid meat-peptone broth for 6 h at 37 °C. The resulting suspensions were then adjusted to an optical density of 0.5 on the McFarland scale, which corresponds to approximately 10^8 colony-forming units (CFU) per cm^3.

The antimicrobial potential of the HDES was evaluated according to the recommendations of the Clinical and Laboratory Standards Institute (CLSI), document M02-A11 (Performance Standards for Antimicrobial Susceptibility Disk Tests). Solutions of the HDES were soaked onto 6 mm diameter disks made of Whatman™ microfiber filters.

The inoculated agar plates were evenly distributed using a sterile swab, after which the soaked disks were carefully placed on the surface. The Petri dishes were incubated at 37 °C for 24 and 48 h. Antibacterial activity was determined by measuring the diameter of the inhibition zones formed around the disks. All experiments were performed in triplicate and the results are reported as mean values.

2.7 Determination Polarity of HDES

The polarity of the HDES was evaluated using Nile red (9-diethylamino-5-benzo[a]phenoxazinone) as a solvatochromic probe (Berry et al. 2015). The method is based on the sensitivity of Nile Red's spectral properties to the polarity of its microenvironment. The Nile Red stock solution was prepared in ethanol at a concentration of 1 mM and then diluted to a concentration of 2×10^{-5} mol L^{-1} before spectral measurements. In a quartz cuvette, 980 µL of HDES and 20 µL of the Nile Red solution (2×10^{-5} mol L^{-1}) were mixed, and the resulting solution was analysed in the visible range (400–700 nm) using a UV–Vis spectrophotometer (Thermo Scientific, Evolution 220). The mixtures were homogenized and equilibrated at 25 ± 1 °C prior to measurement. UV–Vis absorption spectra were recorded in the range of 350–650 nm using quartz cuvettes with a 1 cm optical path length. The emission maximum (λ_{max}) of Nile Red in each HDES was determined and compared with those obtained in reference solvents of known polarity (ethanol, and water). All measurements were performed in triplicate, and the reported values represent the mean ± standard deviation. The maximum absorption wavelength (λ_{max}) corresponding to the intramolecular charge transfer band was

identified. The Normalized Reichardt polarity parameter E_T^N was calculated according to Eq. (1):

$$E_T^N = \frac{28591}{\lambda_{\max}} \tag{1}$$

where E_T^N (kcal/mol) is Normalized Reichardt polarity parameter, λ_{max} (nm) is maximum absorption wavelength.

For Nile Red was calculated according to Eq. (2)

$$\pi^* \approx 0.938 \cdot \frac{E_T^N}{100} \tag{2}$$

where π^* is dimensionless dipolarity/polarizability scale.

This is a rough conversion from E_T^N (kcal/mol) to the dimensionless dipolarity/polarizability scale (0–1.2).

2.8 Determination of the Surface Tension

The surface tension components of HDES were determined using the combined approach. At first, total surface tension of HDES was determined then its diperse component and the polar component was calculated as follows. The total surface tension $\gamma_L\ (N/m)$ was characterized with the approach described in detail in (Ivanova et al. 2025; An and Row 2021) with the pendant drop method using the Worthington criteria ($W_o \geq 0.6$) of data validation. The pendant drop tensiometry is based on the following Eq. 3:

$$B_o = \frac{\Delta\rho \times g \times R_0^2}{\gamma_L} \tag{3}$$

where B_o is the Bond number, a coefficient that describes the curvature of the pendant droplet surface, $\Delta\rho\ (kg/m^3)$ is the difference between the density of droplet liquid and surrounding environment, $g\ (N/kg)$ is the gravitational acceleration, R_0 (m) is the radius of the droplet, $\gamma_L\ (N/m)$ is the surface tension of analysed liquid.

The validation of the result is possible with Worthington criteria (Eq. 4):

$$W_o = \frac{\Delta\rho \times g \times V_d}{\gamma_L \times D_n} \tag{4}$$

where W_o is Worthington criteria, $V_d\ (L)$ is the actual droplet volume; $D_n\ (m)$ is the needle outer diameter. As it was shown in (Langhals 2023), the measurement is valid in case if Worthington criteria value is ≥0.6.

To obtain pendant droplet images the BGD-190 (Bigued Precision instruments, PRC) tensiometer was used. Images were processed with open-source One Drop software reported in (Langhals 2023), that calculated B_o and W_o numbers on the base of droplet geometry and input of density difference, needle diameter and the image scale.

The next step was the obtaining of the surface tension components values. Disperse $\gamma_L^D(mJ/m^2)$ and polar $\gamma_L^p(mJ/m^2)$ components of the surface tension of liquids were considered as the summands of the total surface tension $\gamma_L\ (mJ/m^2)$ (Eq. 5):

$$\gamma_L = \gamma_L^D + \gamma_L^p \tag{5}$$

The value of $\gamma_L^D\ (mJ/m^2)$ was determined using the reduced Fowkes approach based on the measurement of the liquid static contact angle on the surface with neglectable value of the polar surface energy component (γ_S^p) ($\gamma_S^p \rightarrow 0$), which was teflon substrate.

In the course of Fowkes theory the solid surface energy (γ_S,) is expressed as $\gamma_s = \gamma_S^D + \gamma_S^p$, where γ_S^D is disperse component of the solid surface energy, γ_S^p is polar surface energy component. To check this assumption, the fraction of the disperse surface energy of this surface was measured with water and cyclohexanone as the probe liquids (they gave the contact angle values 113° and 30° respectively) in the scope of OWRK calculation (automatically with Shengding 4.0 software of tensiometer) and it was found that solid surface energy of PTFE γ_S = 22,8 mJ/m^2, γ_S^p = 0,2 mJ/m^2 and γ_S^D=22,6 mJ/m^2 respectively, so the value of the polar component was found within an error margin and it can be concluded that $\gamma_S \approx \gamma_S^D$.

The reduced Fowkes equation (Eq. 6) links this value, the obtained contact angle (θ) and the total surface tension of the liquid γ_L with its disperse fraction γ_L^D:

$$\gamma_L(1+\cos\theta) = 2 \times \sqrt{\gamma_L^D \times \gamma_S} \tag{6}$$

Using an Eq. 5 (Eq. 5) and the obtained value of the disperse component of the liquid surface tension, the polar component was determined.

2.9 Separation of Methylene Blue and Diclofenac from Aqueous Solutions Using HDES

The extraction performance of the synthesized HDES was assessed using a dispersive liquid–liquid microextraction (DLLME) procedure with an aqueous solution of methylene blue (MB) at an initial concentration of 100 ppm. An aliquot of 20 µL of HDES was rapidly injected into 1 mL of the aqueous MB solution, followed by agitation using a magnetic stirrer at 800 rpm for 20 min to promote the formation of a homogeneous cloudy dispersion and enhance mass transfer between phases. All experiments were performed at a controlled ambient temperature of 20±1 °C to account for the temperature-dependent viscosity of menthol-based HDES. Subsequently, the mixture was centrifuged at 6000 rpm for 5 min to ensure complete phase separation. The HDES-rich phase and the aqueous phase were carefully separated using a microsyringe. The residual concentration of MB in the aqueous phase was determined by UV–Vis spectrophotometry at a maximum absorbance wavelength of 665 nm. All experiments were performed in triplicate, and the results are presented as mean values ± standard deviation.

The extraction performance of the prepared HDESs toward diclofenac (DIC) was evaluated using an aqueous solution with an initial concentration of 40 mg L^{-1}. In a typical experiment, 2 mL of HDES was added to 5 mL of the DIC solution, followed by vortex-assisted

mixing at 2500 rpm for 20 min to ensure efficient dispersion and mass transfer between phases. All experiments were conducted at a controlled ambient temperature of 20 ± 1 °C to account for the temperature-dependent physicochemical properties (e.g., viscosity) of menthol-based HDES. After extraction, phase separation was achieved by centrifugation at 2000 rpm for 10 min. This resulted in the formation of a distinct HDES-rich phase containing the extracted analyte, which accumulated in the upper layer. The aqueous phase was carefully removed using a syringe to avoid cross-contamination. The residual concentration of DIC in the aqueous phase was determined by UV–Vis spectrophotometry at a wavelength of 276 nm. All measurements were carried out in triplicate, and the results are reported as mean values with standard deviations. The Extraction Efficiency (*EE*, %) was calculated using the following Eq. 7:

$$EE\ (\%) = \frac{C_{ic} - C_{ec}}{C_{ic}} \times\ 100 \tag{7}$$

where C_{ic} is the initial concentration of MB (mg/L) or DIC (mg/L) and C_{ec} is the equilibrium concentration of the MB or DIC in the aqueous phase after extraction.

2.10 Determination of HBD Leaching from HDES During Dispersive Liquid–Liquid Microextraction (DLLME)

To assess the potential leaching of the hydrogen bond donor (HBD) from the (HDES during dispersive liquid–liquid microextraction (DLLME), the water solubility of the HDES and the acid content in the aqueous phase were evaluated. For the solubility test, a known volume of HDES (5 mL) was added to deionized water (5 mL) and vortexed to ensure thorough mixing (10 min). After allowing the system to reach equilibrium, the aqueous phase was separated by centrifugation and analyzed to determine the concentration of the acid. The analysis was performed by acid–base titration (0.01 M NaOH). The extent of HBD leaching was calculated as the percentage of acid present in the aqueous phase relative to the initial amount in the HDES using the following Eq. 8.

$$\text{Leaching}\,(\%) = \frac{m_{\text{acid, aq}}}{m_{\text{acid, HDES}}} \times\ 100 \tag{8}$$

Low leaching (< 5–10%) indicates the HDES maintains its integrity during extraction, whereas higher leaching (> 10%) suggests a change in the DES molar ratio, potentially affecting extraction efficiency. Low leaching indicated that the HDES largely maintained its original molar ratio during the extraction, confirming its stability and suitability for DLLME applications.

2.11 Statistical Analysis

All measurements were performed with triplicate samples and the results are reported as mean ± standard deviation. Statistical analysis was performed by ANOVA using SPSS statistical software (IBM, USA). P value < 0.05 is considered significant.

3 Results and Discussion

3.1 Predictive Assessment of Reactivity Based on Quantum Chemical Calculations

To predict the efficiency of HDES formation, quantum chemical parameters such as molecular electrostatic potential (MEP) maps, HOMO–LUMO energies, and global reactivity descriptors are particularly informative (Shah et al. 2025; Guidugli and Reza 2025; Chen et al. 2025). MEP analysis provides insight into the distribution of electron density across the molecules, allowing the identification of regions with positive and negative electrostatic potential that act as hydrogen bond donors and acceptors. This is crucial for understanding the non-covalent interactions (hydrogen bonding, dipole–dipole, and van der Waals forces) responsible for HDES formation. Meanwhile, frontier molecular orbitals (HOMO and LUMO) and their energy gap (ΔE = E LUMO – E HOMO) describe the molecule's ability to donate or accept electrons, reflecting its chemical reactivity and stability. Complementary global descriptors such as electronegativity (χ), chemical potential (μ), hardness (η), softness (S), and electrophilicity (ω) further quantify these tendencies and enable comparative assessment of potential component pairs (Guidugli and Reza 2025; Cysewski et al. 2025; Chen et al. 2025; Shakourian-Fard et al. 2021; Singh et al. 2024; Zheng et al. 2025a, b). Formulas for calculation are presented in supplementary material (Section SM1). Together, these parameters provide a reliable theoretical framework for predicting and rationalizing the strength and directionality of intermolecular interactions in hydrophobic DES systems, where classical ionic interactions are largely replaced by weak hydrogen bonding and dispersion forces.

3.2 Prediction of DES Formation via MEP Analysis

The current work displays the MEP surface of levulinic acid, acetic acid, lactic acid, oleic acid, linalool in Fig. 1. MEP — regions of positive/negative potential for predicting binding sites (H-bond donors/acceptors). MEP maps represent the distribution of electrostatic potential on the molecular surface, where red regions indicate electron-rich (nucleophilic) sites and blue regions indicate electron-deficient (electrophilic) sites. This visualization helps identify potential sites for hydrogen bonding and other noncovalent interactions between HDES components. The molecular electrostatic potential (MEP) map of menthol reveals an uneven charge distribution associated with its functional groups (Kumar et al. 2024; Guidugli and Reza 2025; Zheng et al. 2025a, b; Rodríguez-Juan et al. 2021). The most negative electrostatic potential regions (depicted in pink) are localized around the oxygen atom of the hydroxyl group, indicating sites with a high electron density capable of acting as hydrogen bond acceptors. In contrast, the most positive potential regions (in green) are concentrated near the hydrogen atom of the hydroxyl group and around the aliphatic hydrogen atoms attached to the carbon skeleton, suggesting possible hydrogen bond donor sites (Cysewski et al. 2025; Chen et al. 2025). The overall MEP pattern reflects the amphiphilic nature of menthol, where the polar hydroxyl group is embedded within a largely nonpolar hydrocarbon framework. This balance between hydrophilic and hydrophobic regions explains menthol's ability to participate in weak hydrogen bonding interactions while maintaining overall hydrophobic character - an important feature for the formation of HDES (Guidugli and

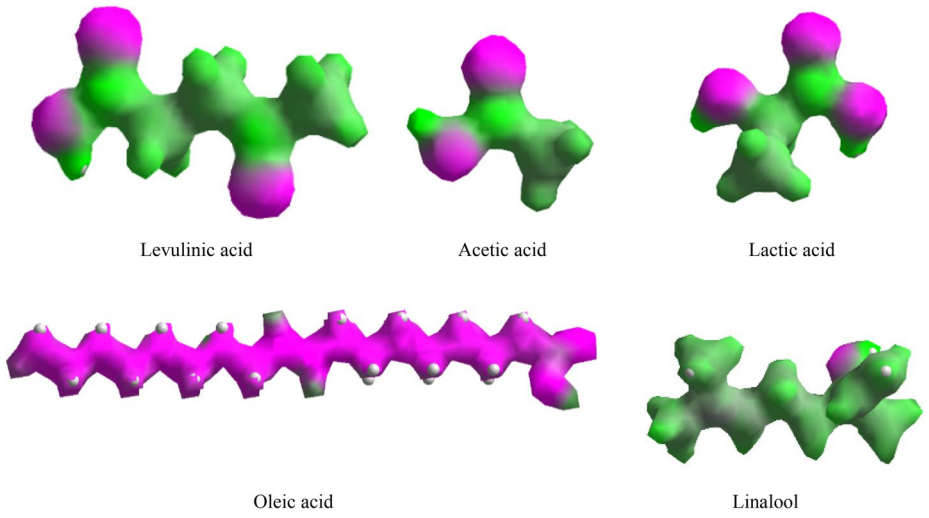

Fig. 1 Molecular electrostatic potential (MEP) surfaces of the studied compounds

Table 2 Calculated minimum and maximum electrostatic potentials (V_{min} and V_{max}) and the resulting ΔV ($V_{max} - V_{min}$) for selected compounds used in HDES systems

Compound	V_{min} (a.u.)	V_{max} (a.u.)	$\Delta V = V_{max} - V_{min}$ (a.u.)
Levulinic acid	−0.129	0.572	0.701
Acetic acid	−0.142	0.656	0.798
Lactic acid	−0.147	0.647	0.794
Oleic acid	−1.07	0.205	1.275
Linalool	−0.151	0.401	0.552

Reza 2025; Cysewski et al. 2025; Chen et al. 2025; Shakourian-Fard et al. 2021; Singh et al. 2024; Zheng et al. 2025a, b; Rodríguez-Juan et al. 2021; Li et al. 2025; Vorobyova 2023).

The MEP analysis of the studied molecules highlights their hydrogen-bonding capabilities, which are critical for HDES formation. Levulinic acid exhibits pronounced negative potential around the ketone and carboxyl oxygens, indicating strong H-bond acceptor sites, while the –OH hydrogen of the carboxyl group acts as a donor (Table 2).

Acetic acid similarly presents negative potential at the carboxyl oxygen and positive potential at the hydroxyl hydrogen, facilitating intermolecular H-bonding and self-association. Lactic acid shows multiple donor and acceptor sites, with negative potential on the hydroxyl and carboxyl oxygens and positive potential on the corresponding hydrogens, enabling extensive hydrogen-bond networks. Oleic acid demonstrates negative potential at the carboxyl group and a positively polarized hydroxyl hydrogen, while its long hydrophobic chain remains neutral, contributing to amphiphilic interactions in HDES. Linalool possesses a localized negative potential at the hydroxyl oxygen and a positive potential at the hydroxyl hydrogen, allowing it to participate in weak H-bonding despite its largely nonpolar structure. Collectively, these MEP profiles indicate that all molecules can act as hydrogen bond donors and/or acceptors, supporting the formation and stabilization of HDES through complementary electrostatic interactions. These patterns suggest that short-chain acids are likely to form more structured and polar hydrogen-bond networks, whereas hydrophobic components are expected to contribute to less polar and more flexible domains.

Consequently, the MEP-derived predictions provide insight into the formation, polarity, and structural organization of the synthesized HDES, supporting their functional behavior in subsequent experimental applications.

3.2.1 Prediction of the Efficiency of HDES Formation by Parameter Based on Frontier Molecular Orbitals (FMO)

The efficiency of HDES formation can be predicted from the frontier orbitals of the components (Vorobyova et al. 2022, 2023; Malik et al. 2022; Shah et al. 2025; Guidugli and Reza 2025; Cysewski et al. 2025; Chen et al. 2025; Shakourian-Fard et al. 2021; Singh et al. 2024; Zheng et al. 2025a, b; Rodríguez-Juan et al. 2021; Li et al. 2025; Vorobyova 2023). Molecules with high HOMO energies act as effective electron donors, while those with low LUMO energies serve as good electron acceptors. Smaller HOMO–LUMO gaps indicate higher reactivity and stronger hydrogen-bonding interactions, facilitating the formation of stable eutectic mixtures (Shakourian-Fard et al. 2021). According to the computed values, the HOMO–LUMO energy gap (ΔE) varies from 10.43 to 12.55 eV among the examined compounds (Tables 3 and 4.). The calculated difference between the maximum and minimum electrostatic potentials ($\Delta V = V_{max} - V_{min}$) serves as a quantitative indicator of molecular polarity and provides insight into the molecule's potential to form hydrogen-bonding interactions within HDES systems (Table 2) (Guidugli and Reza 2025; Cysewski et al. 2025; Chen et al. 2025; Shakourian-Fard et al. 2021). From these results, it is evident that oleic acid exhibits the largest ΔV, suggesting it has a pronounced polarity difference across the molecule, which may influence its solvation behavior despite being hydrophobic. Linalool, with the smallest ΔV, shows the least polarity variation, indicating a lower potential for strong hydrogen-bonding interactions within HDES. The remaining acids (levulinic, acetic, lactic) display intermediate ΔV values, consistent with their ability to participate in hydrogen-bonding interactions while maintaining moderate polarity.

Such a difference reflects the varying stabilities and reactivities of the molecules. Generally, a smaller ΔE value indicates a greater ability of the molecule to participate in electron transfer and chemical reactions, since the excitation of electrons requires less energy. Levulinic acid exhibited a HOMO–LUMO gap of 11.42 eV and the highest electrophilicity index ($\omega = 2.42$ eV). This suggests that it is the strongest electrophile among the studied compounds, showing a high propensity to accept electrons in intermolecular interactions. Its chemical hardness ($\eta = 5.71$ eV) and negative chemical potential ($\mu = -5.26$ eV) also support its intermediate stability and tendency to undergo polar reactions. Acetic and lactic acids, on the other hand, showed the largest hardness values (6.28 and 6.09 eV, respectively) and relatively high ionization energies (11.61 and 11.24 eV).

These parameters indicate that the small carboxylic acids are relatively chemically stable and less reactive, requiring higher energy for electron removal or excitation, as reflected in their higher HOMO–LUMO gaps (12.55 and 12.18 eV) and lower electrophilicity indices (2.26 and 2.18 eV). In contrast, oleic acid and linalool exhibit slightly smaller HOMO–LUMO gaps (10.76 and 10.43 eV) and lower chemical hardness values (5.38 and 5.22 eV), suggesting a greater tendency for electronic interaction within HDES networks rather than absolute chemical reactivity. These trends correlate qualitatively with their behavior in HDES formation, polarity modulation, and functional performance, including extraction efficiency and antibacterial activity.

Table 3 Quantum chemical parameters of the optimized compounds

Compound	EHOMO (eV)	ELUMO (eV)	ΔE (ELUMO−EHOMO), eV	IE = − EHOMO	EA = − ELUMO	Chemical potential (μ)	Chemical hardness (η)	Global electrophilicity index (ω)
Levulinic acid	−10.9707	0.4464	11.4171	10.9707	−0.4464	−5.2622	5.7085	2.42
Acetic acid	−11.6062	0.9444	12.5506	11.6062	−0.9444	−5.3309	6.2753	2.26
Lactic acid	−11.2377	0.9396	12.1773	11.2377	−0.9396	−5.1491	6.0887	2.18
Oleic acid	−9.8037	0.9585	10.7621	9,8037	−0.9585	−4.4226	5.3811	1.82
Linalool	−9.5938	0.8384	10.4323	9.5938	−0.8384	−4.3777	5.2161	1.84

These findings are consistent with the molecular structure of these compounds: both contain extended hydrocarbon chains and π-systems that favor charge delocalization, facilitating orbital interactions with other species. The low hardness of linalool, combined with its moderate electrophilicity (1.84 eV), suggests that it can readily participate in soft–soft interactions, such as hydrogen bonding and π–π stacking, which are important in supramolecular or solvent–solute systems (Chen et al. 2025).

From the viewpoint of global reactivity trends, the results indicate that Levulinic acid behaves as the strongest electrophile, Linalool is the most chemically "soft" and thus the most reactive and fcetic acid is the most chemically inert compound in the studied series. In summary, the comparative analysis demonstrates that the reactivity order based on electrophilicity and chemical softness follows: Levulinic acid > Lactic acid ≈ Acetic acid > Oleic acid > Linalool (electrophilicity trend) and Linalool > Oleic acid > Levulinic acid > Lactic acid > Acetic acid (softness/reactivity trend).

These findings highlight the distinct electronic behaviors of the molecules, which can be important for predicting their hydrogen-bonding ability, electron transfer characteristics, and potential interaction as hydrogen-bond donors in eutectic solvent systems or catalytic media.

3.3 Structural Characterization of HDES by NMR and FTIR

The structural characterization of HDES composed of menthol and levulinic acid was performed using proton (^{1}H) and carbon (^{13}C) nuclear magnetic resonance spectroscopy (Section SM2, Fig. SM1). The spectra were recorded at 25 °C in $CDCl_3$ as solvent. In the ^{1}H NMR spectrum, the characteristic signals of menthol were observed at δ 0.80–1.10 ppm (m, CH_3 groups), 1.20–1.90 ppm (m, aliphatic CH_2), 3.35 ppm (m, CH–OH), and 4.45 ppm (br s, OH). Levulinic acid exhibited resonances at δ 2.10 ppm (s, CH_2 adjacent to carbonyl), 2.65 ppm (t, CH_2–COOH), and 11.90 ppm (br s, carboxylic OH). In the HDES spectrum, a noticeable downfield shift of the hydroxyl proton of menthol and the carboxylic proton of levulinic acid was observed, indicating the formation of hydrogen bonds between the –OH group of menthol (hydrogen bond donor) and the C=O or –COOH group of levulinic acid (hydrogen bond acceptor). This interaction confirms the establishment of a eutectic-type supramolecular structure. The ^{13}C NMR spectrum of the HDES revealed the characteristic signals of both components: δ 14–35 ppm (menthol aliphatic carbons), 40–50 ppm (C–OH of menthol), 29.7 and 37.5 ppm (CH_2 of levulinic acid), 177.8 ppm (C=O of carboxylic acid), and 205.5 ppm (C=O of ketone group). Slight chemical shift variations compared to the spectra of pure components further supported the formation of specific hydrogen-bond interactions and rearrangement of the electronic environment around the carbonyl carbons. The combined NMR results confirm that menthol and levulinic acid interact through hydrogen bonding to form a stable eutectic system with a distinct chemical environment compared to the individual components (An and Row 2021; Liu et al. 2025; Ribeiro et al. 2015; Quaid and Reza 2023; Ojeda et al. 2025; Pachernegg et al. 2024).

The structural characterization of the HDES composed of menthol–acetic acid was performed using proton (^{1}H) and carbon (^{13}C) nuclear magnetic resonance spectroscopy (Section SM2, Fig. SM2). In the ^{1}H NMR spectrum, the characteristic resonances of menthol appeared at δ 0.80–1.10 ppm (m, CH_3), 1.20–1.90 ppm (m, CH_2), 3.35 ppm (m, CH–OH), and 4.45 ppm (br s, OH). For acetic acid, a singlet at δ 2.10 ppm corresponding to

Table 4. HOMO and LUMO orbital distributions and electrostatic potential (ESP) of the molecules used as hydrogen bond donors (HBDs)

Compound	E_{HOMO} (eV)	E_{LUMO} (eV)	Molecular electrostatic potential (MEP)
Levulinic acid	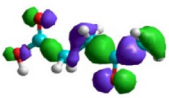	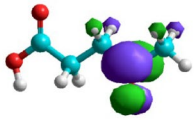	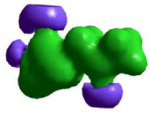
Acetic acid	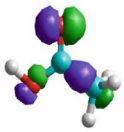	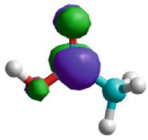	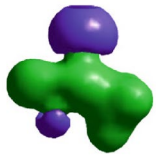
Lactic acid	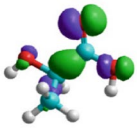	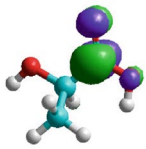	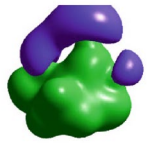
Oleic acid	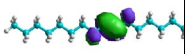		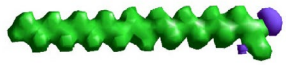
Linalool	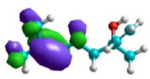	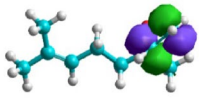	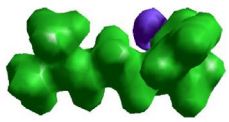

the methyl group (CH_3–COOH) and a broad signal at δ 11.6 ppm (carboxylic OH) were observed. Upon formation of HDES, a downfield shift and broadening of both hydroxyl and carboxylic proton signals were detected, indicating hydrogen bond formation between the hydroxyl group of menthol (hydrogen bond donor) and the carbonyl oxygen of acetic acid (hydrogen bond acceptor) (Ojeda et al. 2025). The ^{13}C NMR spectrum exhibited signals corresponding to menthol at δ 14–35 ppm (aliphatic C), and 40–50 ppm (C–OH), while acetic acid showed a resonance at δ 20.8 ppm (CH_3–COOH) and 178.5 ppm (C = O). Slight chemical shift variations in the HDES spectrum relative to the pure components further confirm the establishment of strong intermolecular hydrogen bonding, leading to the formation of a stable eutectic-type supramolecular structure. The NMR data collectively demonstrate that menthol and acetic acid form a hydrogen-bonded complex, stabilizing the eutectic mixture and creating a distinct chemical environment compared to the individual substances.

The structural characterization of the HDES composed of menthol–lactic acid was performed using proton (^{1}H) and carbon (^{13}C) nuclear magnetic resonance spectroscopy (Section SM2, Fig. SM3). In the ^{1}H NMR spectrum, characteristic signals of menthol appeared at δ 0.80–1.10 ppm (m, CH_3), 1.20–1.90 ppm (m, CH_2), 3.35 ppm (m, CH–OH), and 4.45 ppm (br s, OH). Lactic acid exhibited a multiplet at δ 1.36 ppm (CH_3–CH–OH), a quartet at δ 4.20 ppm (CH–OH), and a broad singlet at δ 11.8 ppm (COOH). Upon formation of the HDES, the hydroxyl and carboxylic protons experienced a downfield shift and broadening, which indicates the formation of hydrogen bonds between the hydroxyl group of menthol (hydrogen bond donor) and the carbonyl or hydroxyl groups of lactic acid (hydrogen bond acceptor). This interaction confirms the establishment of a eutectic-type hydrogen-bonded network (Ribeiro et al. 2015). The ^{13}C NMR spectrum of the HDES revealed characteristic signals of menthol at δ 14–35 ppm (aliphatic carbons) and 40–50 ppm (C–OH), while lactic acid showed signals at δ 20.5 ppm (CH_3), 68.2 ppm (CH–OH), and 178.4 ppm (C=O of carboxylic acid). Slight downfield shifts of carbon resonances compared with the pure components confirm the reorganization of the electronic environment due to intermolecular hydrogen-bond interactions. The combined NMR results provide clear evidence that menthol and lactic acid form a stable deep eutectic mixture stabilized by strong hydrogen bonding between hydroxyl and carboxyl functionalities, which leads to a new supramolecular arrangement and distinct physicochemical behavior compared to the individual substances.

The structural characterization of the HDES composed of menthol–oleic acid was performed using proton (^{1}H) and carbon (^{13}C) nuclear magnetic resonance spectroscopy (Section SM2, Fig. SM4). In the ^{1}H NMR spectrum, menthol displayed characteristic resonances at δ 0.80–1.10 ppm (m, CH_3), 1.20–1.90 ppm (m, CH_2), 3.35 ppm (m, CH–OH), and 4.45 ppm (br s, OH). Oleic acid exhibited signals at δ 0.88 ppm (t, terminal CH_3), 1.25–1.35 ppm (broad m, $(CH_2)_n$ chain), 1.95–2.10 ppm (m, allylic CH_2–CH=CH–CH_2), 2.30 ppm (t, CH_2–COOH), 5.30 ppm (m, olefinic CH=CH), and a broad singlet at δ 11.8 ppm (COOH) (Mannu et al. 2025). In the HDES spectrum, downfield shifts and broadening of the hydroxyl (menthol) and carboxylic (oleic acid) proton resonances were observed, indicating the formation of strong hydrogen bonds between the hydroxyl group of menthol (hydrogen bond donor) and the carbonyl oxygen of oleic acid (hydrogen bond acceptor). The signals of aliphatic and olefinic protons remained largely unchanged, confirming that the interaction primarily involves polar functional groups. The ^{13}C NMR spectrum of the HDES showed characteristic carbon resonances of menthol at δ 14–35 ppm (aliphatic carbons) and 40–50 ppm (C–OH). For oleic acid, the signals appeared at δ 14.1 ppm (CH_3), 22.8–34.5 ppm (aliphatic CH_2 chain), 130.0 ppm (C=C), and 179.2 ppm (C=O). Slight shifts in the carbonyl and carbinol carbon signals relative to pure components confirmed the establishment of specific hydrogen-bonding interactions and the formation of a stable supramolecular eutectic system. Overall, NMR data confirm that menthol and oleic acid form a hydrophobic HDES through hydrogen bonding between –OH and –COOH groups, resulting in a stable and viscous liquid with modified electronic and structural environments compared to the individual components.

The structural characterization of the HDES composed of menthol–linalool acid was performed using proton (^{1}H) and carbon (^{13}C) nuclear magnetic resonance spectroscopy (Section SM2, Fig. SM5). In the ^{1}H NMR spectrum, menthol exhibited its characteristic signals at δ 0.80–1.10 ppm (m, CH_3), 1.20–1.90 ppm (m, CH_2), 3.35 ppm (m, CH–OH), and 4.45 ppm (br s, OH). Linalool showed signals at δ 1.25 ppm (d, CH_3–CH–OH), 1.65 ppm

(s, CH_3 attached to C=C), 5.05 ppm (m, CH_2=CH–), 5.95 ppm (m, CH=CH_2), and 3.45 ppm (m, CH–OH). Upon formation of the HDES, the hydroxyl protons of both components underwent a noticeable downfield shift and broadening, suggesting hydrogen-bond interactions between the hydroxyl groups of menthol and linalool. The ^{13}C NMR spectrum of the HDES showed resonances of menthol at δ 14–35 ppm (aliphatic carbons) and 40–50 ppm (C–OH), while linalool displayed signals at δ 17.6 ppm (CH_3–C=), 25–32 ppm (CH_2), 59.8 ppm (C–OH), 109.3 ppm and 146.8 ppm (C=C).

The slight downfield shift of the carbon atoms bonded to hydroxyl groups indicates the formation of intermolecular hydrogen bonds and slight rearrangement in the electronic environment of both molecules. The NMR data confirm that the menthol–linalool system forms a hydrophobic deep eutectic solvent stabilized by hydrogen bonding between the hydroxyl functionalities of both terpenoid components, leading to the formation of a liquid phase with enhanced miscibility and modified polarity compared to the pure substances. The menthol – levulinic acid HDES exhibited a broad O–H stretching band at ~3330 cm^{-1}, indicative of strong hydrogen-bond formation between the hydroxyl group of menthol and the carbonyl/carboxyl groups of levulinic acid (Fig. 2a). The C=O stretching vibration of the levulinic acid moiety appeared at ~1735 cm^{-1}, slightly shifted and broadened compared to the pure acid, confirming hydrogen-bond interactions. Aliphatic C–H stretching vibrations were observed at 2925–2850 cm^{-1}, while C–O and C–O–H vibrations appeared in the 1180–1045 cm^{-1} region, further supporting the presence of an intermolecular hydrogen-bonded network characteristic of the HDES. The menthol–acetic acid HDES showed a broad O–H stretching band around 3340 cm^{-1}, indicative of strong hydrogen bonding between menthol hydroxyl and acetic acid carboxyl groups (Fig. 2b). The C=O stretching vibration of acetic acid appeared at ~1715 cm^{-1}, slightly shifted and broadened compared to the pure acid, confirming hydrogen-bond interactions. Aliphatic C–H stretching bands were observed at 2925–2850 cm^{-1}, while C–O stretching vibrations appeared in the 1185–1040 cm^{-1} region, supporting the formation of a hydrogen-bonded network characteristic of this HDES. The.

Menthol–lactic acid HDES exhibited a broad O–H stretching band at ~3330 cm^{-1}, indicating strong hydrogen-bond formation between the hydroxyl group of menthol and the hydroxyl/carboxyl groups of lactic acid (Fig. 2c). The C=O stretching vibration of the lactic acid moiety appeared at ~1730 cm^{-1}, slightly shifted and broadened compared to pure lactic acid, confirming intermolecular hydrogen bonding. Aliphatic C–H stretching vibrations were observed at 2925–2850 cm^{-1}, while C–O and C–O–H vibrations in the 1180–1045 cm^{-1} region further support the formation of a hydrogen-bonded network characteristic of this HDES.

The menthol–oleic acid HDES showed a broad O–H stretching band at ~3330 cm^{-1}, indicating strong hydrogen-bond interactions between the hydroxyl group of menthol and the carboxyl group of oleic acid. The C=O stretching vibration of the oleic acid moiety appeared at ~1710–1725 cm^{-1}, slightly shifted and broadened, confirming hydrogen-bond formation. Aliphatic C–H stretching vibrations were observed at 2925 and 2854 cm^{-1}, while C=C stretching (~1650 cm^{-1}) and =C–H stretching (~3005 cm^{-1}) indicate the presence of the cis-alkene in oleic acid. C–O and C–O–H vibrations in the 1180–1040 cm^{-1} region further support the hydrogen-bonded network characteristic of this HDES (Fig. 2d).

The menthol–linalool HDES exhibited a broad O–H stretching band at ~3325–3340 cm^{-1}, indicative of hydrogen-bond formation between the hydroxyl group of menthol and the hydroxyl group of linalool (Fig. 2e). Aliphatic C–H stretching vibrations appeared at

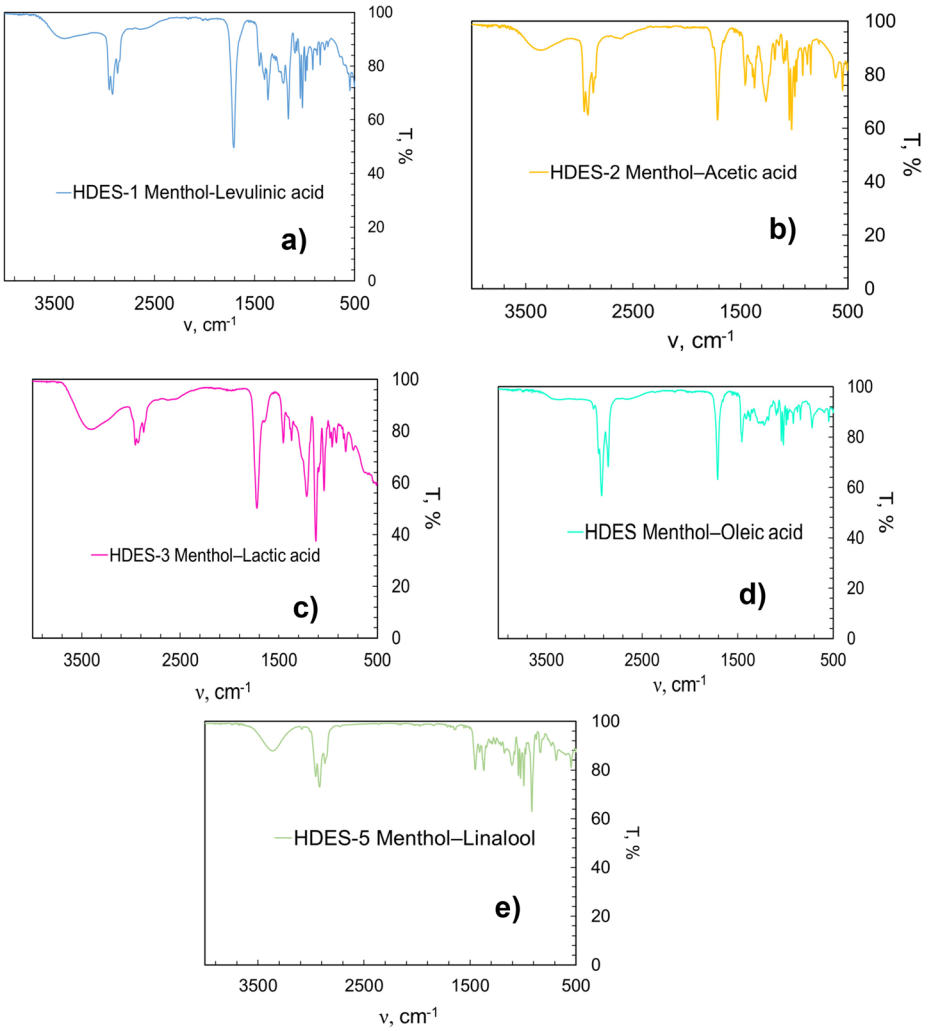

Fig. 2 FTIR spectra of the synthesized HDES

2925–2850 cm^{-1}, while the C–O stretching of alcohol groups was observed in the 1180–1040 cm^{-1} region. The spectral shifts and broadening compared to the pure components confirm the establishment of a hydrogen-bonded network in this HDES.

3.4 Determining the Polarity of HDES

The solvatochromic measurements of Nile Red were used to estimate the polarity of various HDESs. The maximum absorption wavelength (λ_{max}) and corresponding E_TN values were calculated to compare the relative polarity of the studied systems (Fig. 3; Table 5).

The polarity of menthol-based HDESs is influenced by the chemical nature of the hydrogen bond donor (Nakhle et al. 2022). HDESs formed with low-molecular-weight carboxylic

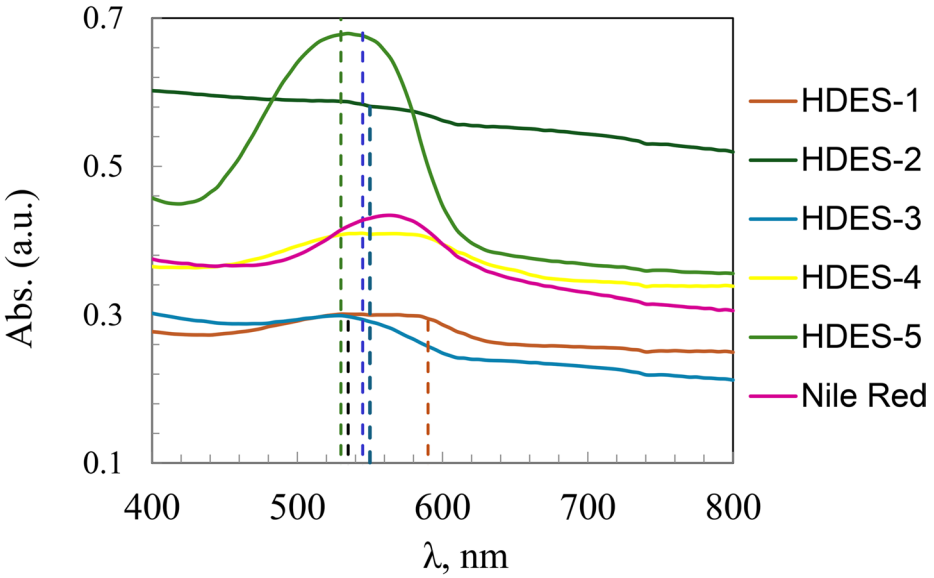

Fig. 3 UV–Vis spectra of Nile red in HDES

Table 5 UV-Vis absorbance maxima (λ_{max}) and E_TN (Nile Red polarity scale) for HDESs

HDES	λ_{max} (nm)	E_TN (kcal·mol^{-1})	π*	α	β
HDES-1	500	53.94	0.51	0.45	0.15
HDES-2	520	57.18	0.54	0.50	0.15
HDES-3	530	53.94	0.51	0.55	0.15
HDES-4	530	52.46	0.49	0.35	0.10
HDES-5	545	54.98	0.52	0.30	0.10

acids (acetic, lactic, and levulinic acids) exhibited comparatively lower E_TN values, reflecting higher polarity due to the presence of polar carboxyl and hydroxyl groups capable of stronger hydrogen-bond interactions. In contrast, HDESs containing hydrophobic or terpene-based donors, such as oleic acid and linalool, showed slightly higher E_TN values, corresponding to reduced solvent polarity. For example, the menthol–linalool HDES displayed one of the highest E_TN values (54.98 kcal·mol^{-1}), indicative of dominant dispersive interactions and comparatively weaker hydrogen-bond donating ability. These results demonstrate that moderate tunability of polarity in menthol-based HDESs can be achieved by selecting hydrogen bond donors with different functional groups and hydrophobicity. Although the numerical differences in E_TN are relatively small, they are consistent with observed trends in solvation behavior, extraction efficiency, and antibacterial activity. Importantly, the prepared systems exhibit hydrophobic behavior, characterized by limited miscibility with water, and their classification as HDES is primarily based on phase behavior in aqueous systems rather than polarity values alone (Nakhle et al. 2022).

The calculated Kamlet–Taft solvatochromic parameters (π*, α, β) for the synthesized menthol-based HDES reveal notable differences in their polarity and hydrogen-bonding properties. HDES-2 exhibits the highest dipolarity (π*), indicating the strongest polarity effect among the studied systems. In contrast, HDES-3 shows the highest HBD acidity

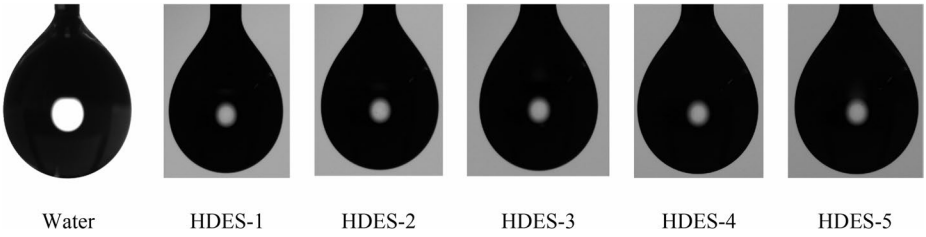

Fig. 4 Pendant droplet images

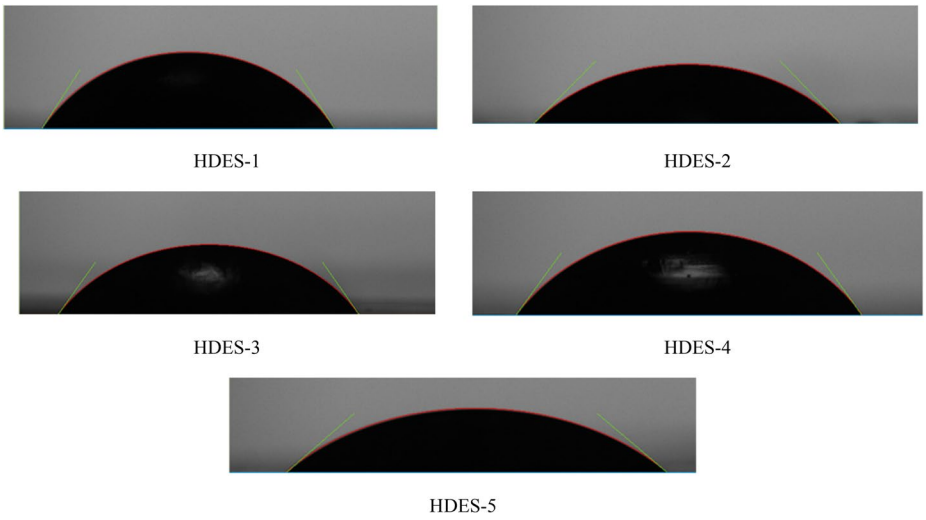

Fig. 5 Contact angles on the PTFE surface

(α), reflecting a greater ability to engage in hydrogen-bonding interactions. HDES-4 and HDES-5 are comparatively more hydrophobic, with lower values of both α and β, suggesting reduced hydrogen-bonding capacity and lower polarity. These differences in solvatochromic parameters are consistent with the nature of the hydrogen bond donors and acceptors in each HDES and help rationalize their behavior in extraction and solvation processes.

3.5 Surface Properties of Menthol-Based HDES

The surface properties of the synthesized menthol-based HDES were systematically investigated, including interfacial tension (IFT) at the HDES–water interface, drop volume (V), surface area (SA), Bond number (Bo), Worthington number (W_o), density (ρ), contact angle on PTFE, and the corresponding total, dispersive, and polar components of the surface energy (Figs. 4 and 5; Table 6). These parameters provide insight into the wettability, spreading behavior, and intermolecular interactions of the HDES.

The interfacial tension (IFT) of the HDES ranged from 36.79 mJ/m² for HDES-1 (menthol–levulinic acid) to 27.68 mJ/m² for HDES-5 (menthol–linalool), significantly lower than that of water (71.35 mJ/m²). This indicates that all HDES exhibit reduced cohesive

Table 6 Total surface tension of HDES

Liquid	IFT, mJ/m^2	V, mm^3	S mm^2	B_o	W_o	ρ, g/cm^3
Water	71.35	9.69	22.23	0.2030	0.8231	0.998
HDES-1	29.87	4.10	12.33	0.2542	0.8129	0.973
HDES-2	28.40	4.176	12.75	0.2548	0.8268	0.925
HDES-3	30.82	3.985	12.26	0.2617	0.8401	1.069
HDES-4	30.19	4.541	13.41	0.2492	0.8243	0.902
HDES-5	27.68	4.26	12.69	0.2515	0.8121	0.877

Table 7 Fractions of the surface energy

Liquid	Contac angle on PTFE	Total	Disperse	Polar
Water	113	71.35	20.90	50.45
HDES-1	54.0	29.87	24.88	4.99
HDES-2	42.3	28.4	27.00	1.40
HDES-3	54.9	30.82	26.07	4.75
HDES-4	52.2	30.19	26.23	3.96
HDES-5	40.5	27.68	26.27	1.41

energy and enhanced spreading at the liquid–liquid interface compared to water, with the lowest IFT observed for systems containing more hydrophobic donors such as linalool and oleic acid.

Drop volume (V) (Fig. 4) and surface area (SA) (Fig. 5) measurements showed only minor variations among the HDES, with drop volumes ranging from 3.985 mm³ to 4.541 mm³ and surface areas from 12.26 mm² to 13.41 mm², reflecting uniform droplet formation and stable liquid behavior. Densities varied from 0.877 g/cm³ (HDES-5) to 1.195 g/cm³ (HDES-1), correlating with the molecular weight and hydrophobicity of the hydrogen-bond donor.

Contact angle measurements on PTFE revealed a strong dependence on HDES composition. HDES-1 (menthol–levulinic acid) exhibited a contact angle of 77.2°, while HDES-5 (menthol–linalool) displayed the lowest angle of 40.5°, in contrast to water at 113° (Table 7). This trend indicates increasing wettability and spreading with more hydrophobic or less polar hydrogen-bond donors.

3.6 Antibacterial Properties of V-Type Menthol-Based HDES

HDES based on menthol are of particular interest due to their potential antibacterial activity. Menthol itself possesses well-documented antimicrobial effects, primarily through disruption of bacterial cell membranes and interference with cellular metabolism. When combined with complementary hydrogen bond donors or acceptors such as organic acids, fatty acids, or phenolic compounds menthol-based HDES can exhibit enhanced antibacterial efficiency. These eutectic systems may act synergistically, improving solubility and penetration of active components into bacterial membranes. As a result, menthol-based HDES are considered promising green antibacterial agents, suitable for use in pharmaceutical, cosmetic, and hygienic formulations, where biocompatibility and low toxicity are essential (Jabbarvand and Jahanbin 2025; Bagović Kolić et al. 2025; Duque et al. 2023).

3.7 Extraction Efficiency of Methylene Blue by HDES

The antibacterial activity of V-type menthol-based HDES was evaluated against selected Gram-positive and Gram-negative bacteria (Fig. 6). The V-type HDES, composed of menthol as the hydrogen-bond acceptor and various hydrogen-bond donors (levulinic acid, acetic acid, lactic acid, oleic acid, and linalool), exhibited significant inhibitory effects, which were influenced by the nature of the donor molecule. HDES containing levulinic acid and lactic, acetic acid showed the strongest antibacterial activity, likely due to their higher polarity and stronger hydrogen-bonding interactions, which enhance solubility and bioavailability of the bioactive menthol component. In contrast, HDES with oleic acid and linalool, being more hydrophobic and less polar, exhibited moderate to lower antibacterial effects. The menthol-based HDES exhibited stronger antibacterial activity against Bacillus subtilis than against Gram-negative strains.

This effect can be attributed to the absence of an outer lipopolysaccharide membrane in B. subtilis, which facilitates the penetration of HDES molecules (Farias et al. 2025; Sanches et al. 2023; Shah et al. 2023; Azmi et al. 2021). The synergistic action of menthol and organic acids further enhances membrane disruption and proton imbalance, leading to increased bacterial susceptibility. The observed antibacterial effect of the menthol–acetic acid HDES was more pronounced against Gram-negative bacteria. This may be attributed to the physicochemical nature of the eutectic system, where the acetic acid component, in its non-dissociated form, can readily penetrate the outer membrane of Gram-negative cells. Once inside, the acid dissociates, leading to intracellular acidification that disrupts enzymatic activity and impairs essential transport processes. In addition, the hydrophobic menthol moiety can interact with the lipid components of the bacterial membrane, increasing its permeability and facilitating acid entry. The combined effect of membrane destabilization and pH imbalance accounts for the stronger inhibitory action of the menthol–acetic acid HDES toward Gram-negative species compared with Gram-positive ones (Silva et al. 2019; Zeng et al. 2021). The lower antibacterial efficiency of the menthol–oleic acid deep eutectic solvent is mainly due to its strong hydrophobicity, poor miscibility with aqueous media, and weak acidity of oleic acid, which together limit its diffusion toward bacterial membranes and prevent intracellular acidification. The high antibacterial activity of the menthol–linalool deep eutectic solvent arises from the synergistic interaction of two bioactive terpenes that strongly disrupt bacterial membrane integrity through lipid solubilization and increased membrane permeability, leading to leakage of cellular contents and cell death.

The results suggest that the synergistic combination of menthol with suitable hydrogen-bond donors in V-type HDES enhances their ability to interact with bacterial cell membranes, disrupt membrane integrity, and inhibit bacterial growth. These findings indicate that V-type menthol-based HDES are promising bioactive solvents with potential applications in pharmaceutical and cosmetic formulations (Zeng et al. 2021) requiring antimicrobial functionality.

The quantum chemical descriptors of HDES components provide a predictive framework linking molecular structure, physicochemical properties, and antibacterial activity. The HOMO–LUMO gap (ΔE) determines molecular reactivity and the efficiency of intermolecular interactions, influencing the stability and availability of bioactive menthol. The electrostatic potential difference (ΔV) reflects polarity and hydrogen-bonding capacity, where moderate ΔV values (as in short-chain acids) promote solubility and penetration

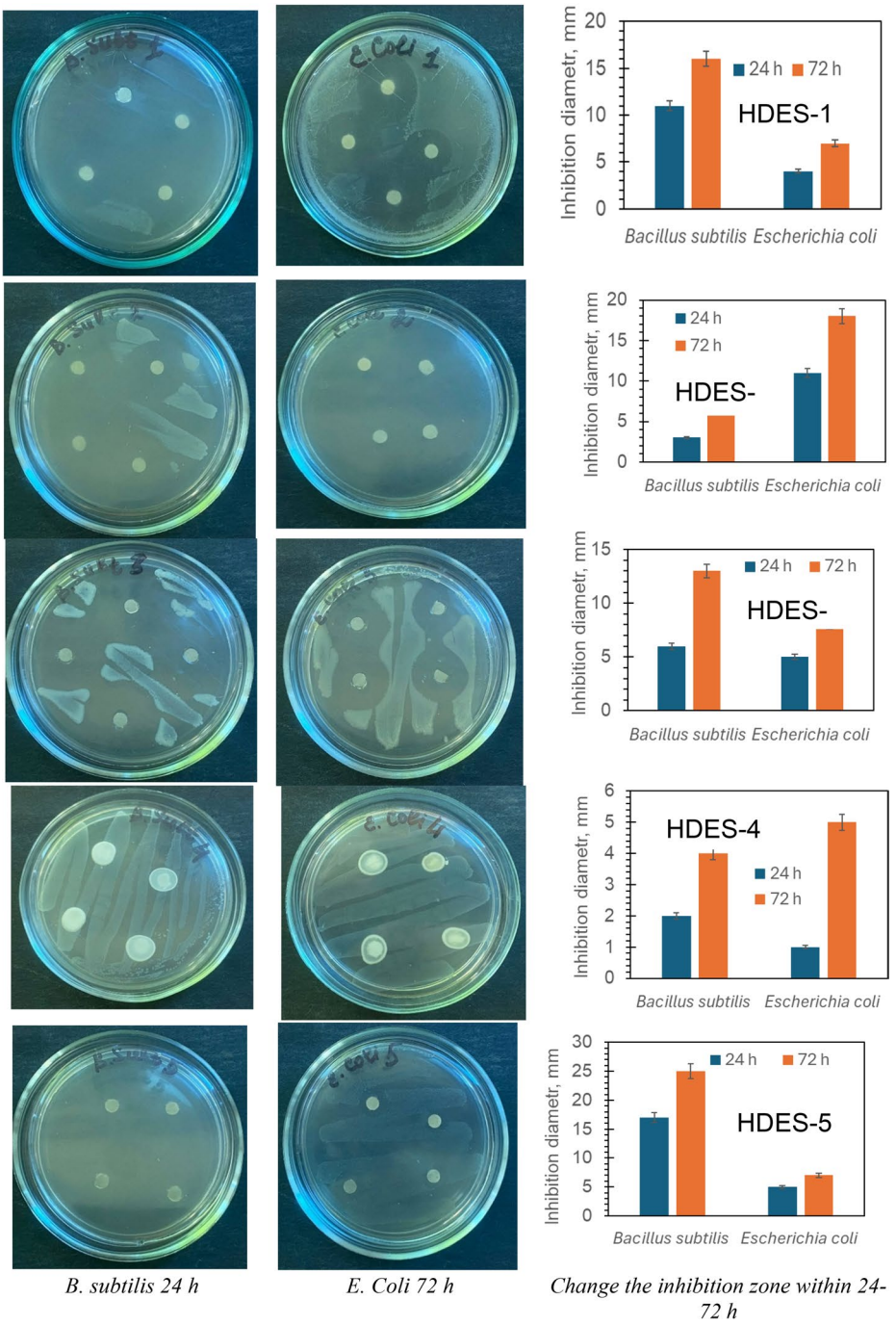

Fig. 6 Representative inhibition zone assay of HDES against Bacillus subtilis (*B. subtilis*) and Escherichia coli (*E. coli*) after 24 and 72 h immersion

into bacterial membranes, while low ΔV values (as in linalool) favor interactions with lipid membranes. Chemical potential (μ) and electrophilicity (ω) govern the tendency of molecules to donate or accept electrons, facilitating proton transfer and intracellular acidification, which disrupts bacterial metabolism.

The type of hydrogen bond donor (acid vs. terpene) further modulates antibacterial mechanisms: acid-based HDES primarily induce intracellular acidification, whereas terpene-rich HDES (menthol–linalool) destabilize bacterial membranes through lipid solubilization. The combined effects of polarity, hydrogen-bonding interactions, and hydrophobicity explain the observed variation in antibacterial efficiency across Gram-positive and Gram-negative bacteria.

The extraction ability of hydrophobic solvents was investigated with respect to the cationic dye methylene blue (MB). When using synthesized HDES, the extraction efficiency varies from 65 to 84% depending on the solvent used (Fig. 7). It is noteworthy that even with an extremely small volume of HDES (20 µl), significant removal of MB from 5 ml of an aqueous solution with a concentration of 100 ppm was sufficient. The mass transfer process is highly efficient and fast, reaching equilibrium within 15 min of contact time. Further increase in the mixing time (up to 60 min) did not significantly change the results, indicating a favorable thermodynamic profile for dye transfer. It was found that the extraction depends on the polarity of the solvent. Visually, the extraction (Fig. 8) resulted in a clear phase separation when using all solvents, where the upper layer of HDES became dark blue (due to the concentrated dye), while the lower aqueous phase became transparent, indicating successful removal of the contaminant (Riyana et al. 2025). Methylene blue (MB) is a cationic dye, it has a significant hydrophobic part, represented by a large aromatic ring. A more non-polar solvent interacts more effectively with this non-polar part of the dye molecule, which contributes to better extraction efficiency.

The extraction efficiency of methylene blue found in this study (65–84%) is broadly consistent with existing literature on hydrophobic deep eutectic solvents used for dye removal from aqueous solutions (Table 8). For example, a thymol–lauric acid HDES achieved near-complete removal of methylene blue (99–100%) under optimized conditions through liquid–liquid extraction, demonstrating the high potential of such hydrophobic solvents for dye remediation (Riyana et al. 2025). Tailored hydrophobic DESs applied in vortex-assisted liquid–liquid microextraction have shown extraction efficiencies close to 99% for methylene blue and other dyes, highlighting the importance of solvent composition and extraction technique (Chen et al. 2025). Fatty acid–based HDES mixtures also achieved high efficiency (~95%) for methylene blue in aqueous microextraction systems, further illustrating the broad applicability of HDES for pollutant extraction. Together, these results support the effectiveness of hydrophobic DESs for dye removal and confirm that solvent polarity, hydrogen-bonding interactions, and extraction method are key factors governing extraction performance.

3.8 Efficiency of Diclofenac Extraction by HDES

The literature reports positive extraction performance of diclofenac sodium (DIC) when using menthol–acetic acid–based hydrophobic deep eutectic solvent, attributed to favorable hydrogen-bonding and hydrophobic interactions. The extraction efficiency of diclofenac was evaluated using a series of HDES based on menthol as the (HBA and various HBD.

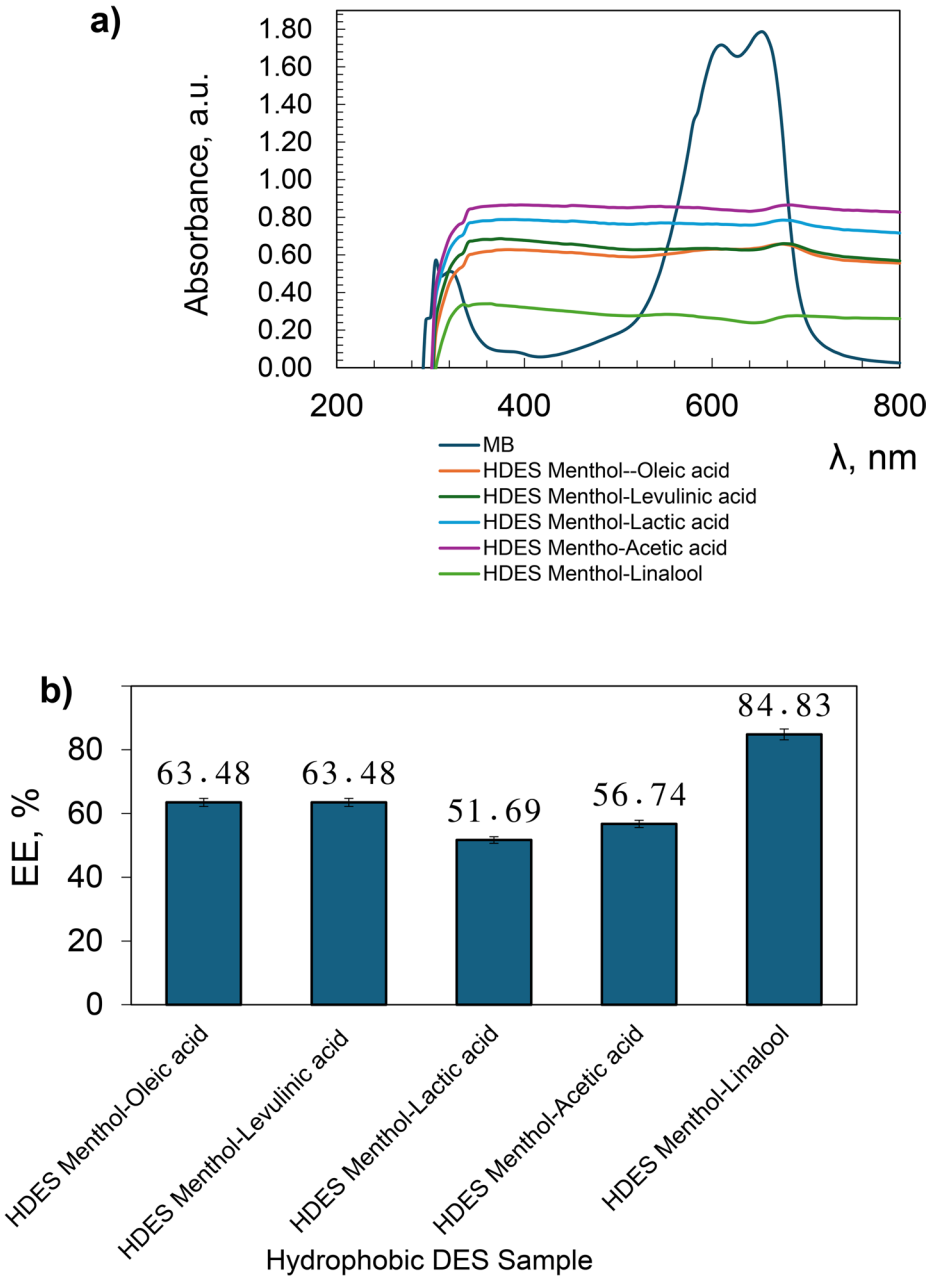

Fig. 7 Efficiency of methylene blue extraction from aqueous solution using HDES: (**a**) UV–Vis spectrum of the aqueous phase after extraction; (**b**) extraction efficiency (EE, %)

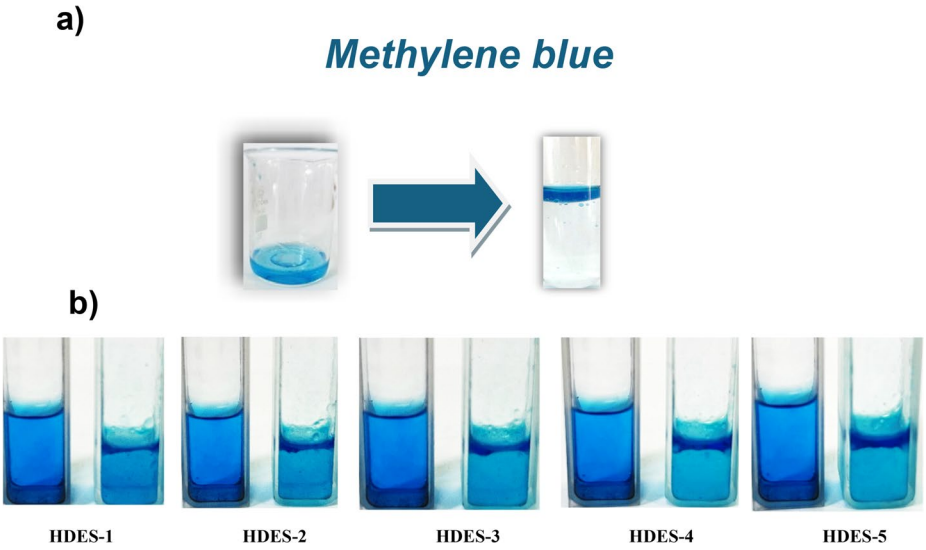

Fig. 8 Methylene blue (MB) solution before extraction (100 ppm) (**a**) and aqueous phase after extraction with 0.7 mL HDES (**b**)

Table 8 Comparison of methylene blue extraction efficiency using different hydrophobic DES from the literature and this study

Solvent system (HDES)	Target compound	Extraction method	Extraction efficiency (%)	Reference
Menthol-based HDES (various HBDs)	Methylene blue	Liquid–liquid extraction	65–84	This study
Thymol–lauric acid	Methylene blue	Liquid–liquid extraction	85–90	Riyana et al. (2025)
Fatty acid-based HDES mixtures	Methylene blue	Micorextraction	~90	Arcon and Franco (2020)
Hydrophobic DES (various compositions)	Methylene blue and dyes	Vortex-assisted microextraction	80 −98	Chen et al. (2025)
Recyclable fatty acid HDES for Sudan dyes	Sudan III/IV (model dyes)	Liquid–liquid extraction	85–90	Siddiqui and Ali (2026)

The tested HBDs included acetic acid, levulinic acid, lactic acid, oleic acid, and linalool. As summarized in Fig. 9., the highest extraction efficiency was observed for the menthol–acetic acid system (52%), due to the small size of acetic acid, its strong hydrogen-bond donating ability, and the low viscosity of the resulting HDES, which facilitates mass transfer. The menthol–levulinic acid (43%) system demonstrated moderate efficiency, likely limited by the higher viscosity and larger molecular size of levulinic acid. Menthol–lactic acid showed lower extraction efficiency, attributed to its hydrophilic character (25%), which may promote water incorporation and reduce diclofenac partitioning. The menthol–oleic acid system was the least effective (7%), as the very hydrophobic and weakly acidic oleic acid provides insufficient hydrogen-bond stabilization of the neutral diclofenac form. Inter-

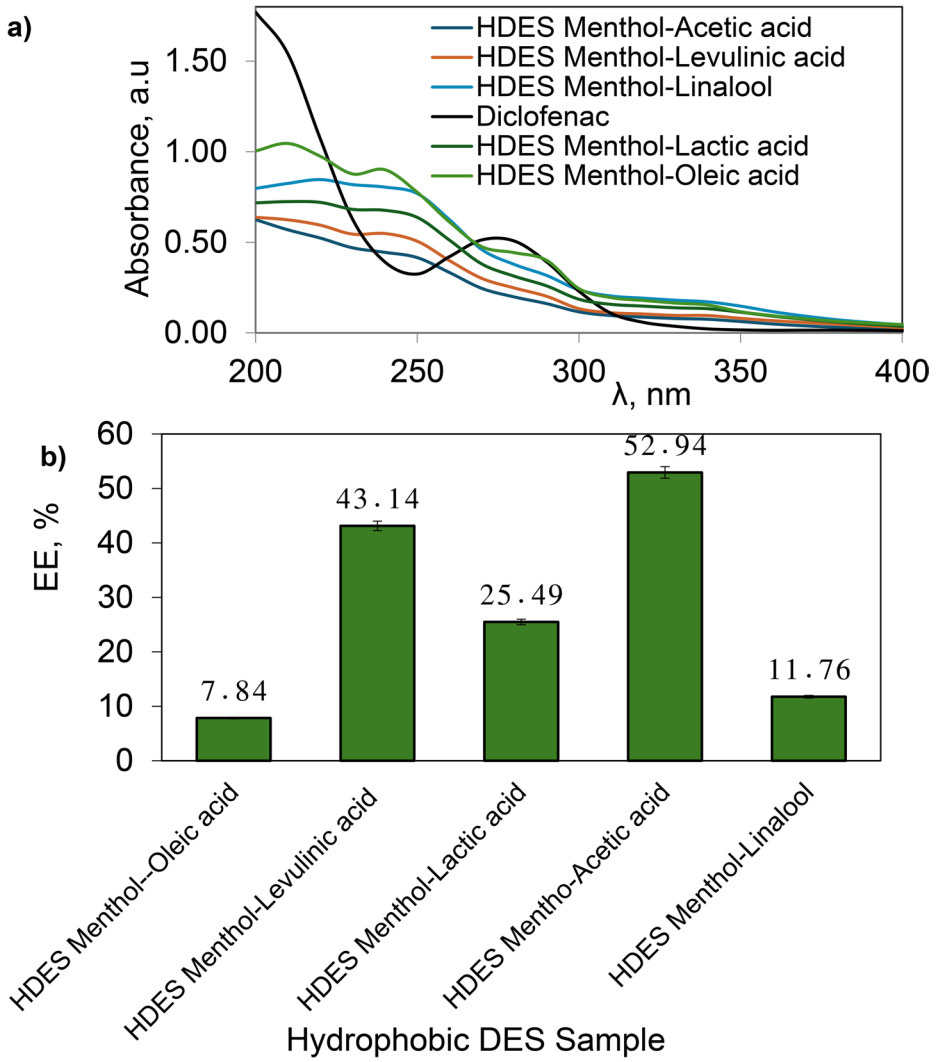

Fig. 9 Efficiency of diclofenac sodium (40 mg/L) extraction from aqueous solution using HDES: (**a**) UV–Vis spectrum of the aqueous phase after extraction; (**b**) extraction efficiency (EE, %)

estingly, linalool, when used as an HBD, exhibited moderate extraction efficiency, slightly lower than acetic acid but higher than oleic acid. The hydroxyl group of linalool provides some hydrogen-bonding interaction with diclofenac, while its hydrophobic terpene skeleton supports partitioning into the HDES phase.

The extent of HBD leaching from menthol-based HDES was quantified by acid–base titration (0.01 M NaOH), and the results are summarized in Section SM3, Table SM1. Leaching strongly depends on the chemical nature of the HBD: HDES-2 (menthol–acetic acid) showed the highest leaching (18.6 ± 0.9%), followed by HDES-3 (menthol–lactic acid, 14.2 ± 0.7%) and HDES-1 (menthol–levulinic acid, 11.5 ± 0.6%). In contrast, hydrophobic systems HDES-4 (menthol–oleic acid) and HDES-5 (menthol–linalool) exhibited minimal

leaching (4.3 ± 0.3% and 2.1 ± 0.2%, respectively). These results confirm that increasing HBD hydrophobicity reduces migration into the aqueous phase, enhancing phase stability and minimizing solvent loss (Marchel et al. 2023).

3.9 Relationship Between Extraction Efficiency and Physicochemical Properties

The extraction efficiency (EE) of the investigated HDES shows a clear dependence on their solvatochromic properties. The highest EE value (84.83%) was observed for the menthol–linalool system (HDES-5), which is characterized by relatively low hydrogen-bond donor acidity (α) and basicity (β), indicating a more hydrophobic environment. This suggests that hydrophobic interactions play a dominant role in the extraction of the dye, enhancing its partitioning into the HDES phase. In contrast, HDES-3 (menthol–lactic acid), which exhibits the highest HBD acidity (α), showed the lowest extraction efficiency (51.69%). This can be attributed to stronger hydrogen-bonding interactions within the solvent network, which reduce the availability of interaction sites for the dye molecules and hinder their transfer. HDES-2 (menthol–acetic acid), despite having the highest dipolarity/polarizability (π*), demonstrated only moderate extraction efficiency (56.74%), indicating that polarity alone is not the determining factor for efficient dye removal. Similarly, HDES-1 and HDES-4, with intermediate solvatochromic characteristics, exhibited comparable EE values (~ 63%), reflecting a balance between polarity and hydrogen-bonding effects.

Overall, the results indicate that lower α and β values combined with moderate π* favor higher extraction efficiency, confirming that reduced hydrogen-bonding capacity and increased hydrophobicity enhance dye removal in these HDES systems.

In contrast to the extraction behavior observed for the dye, the removal efficiency of diclofenac exhibits a different dependence on the solvatochromic parameters of the HDES. The highest extraction efficiency was achieved for HDES-2 (menthol–acetic acid, 52.94%) and HDES-1 (menthol–levulinic acid, 43.14%), which are characterized by relatively higher dipolarity (π*) and moderate hydrogen-bond donor acidity (α). This indicates that, for diclofenac, polar interactions and specific hydrogen bonding play a more significant role in the extraction process. Diclofenac, being a weakly acidic and partially ionizable compound with aromatic structure, can participate in both dipole–dipole interactions and hydrogen bonding. Therefore, HDES systems with balanced π* and α values provide favorable conditions for its solvation and transfer into the eutectic phase. In contrast, HDES-5 (menthol–linalool), which demonstrated the highest efficiency for dye extraction, showed significantly lower extraction efficiency for diclofenac (11.76%). This can be attributed to its low α and β values and predominantly hydrophobic nature, which limits specific interactions with the diclofenac molecule. Similarly, HDES-4 (menthol–oleic acid), with low polarity and hydrogen-bonding ability, exhibited the lowest efficiency (7.84%). HDES-3 (menthol–lactic acid) showed intermediate behavior (25.49%), likely due to its high α value, which may lead to strong internal hydrogen-bonding networks that reduce the availability of interaction sites for diclofenac. Thus, these results suggest that diclofenac extraction is governed by a combination of dipolarity (π) and hydrogen-bond donor ability (α), rather than hydrophobicity*, highlighting a different extraction mechanism compared to the dye.

The obtained results indicate that menthol-based HDES can act as multifunctional systems combining extraction efficiency with intrinsic antimicrobial activity. Depending on their solvatochromic properties, more polar systems favor the removal of polar contami-

nants, while hydrophobic HDES enhance the extraction of nonpolar compounds, simultaneously contributing to bacterial inactivation. This dual functionality highlights their potential as sustainable media for combined extraction and disinfection processes.

3.10 Environmental Assessment of the Use of HDES for Extraction in the Context of Sustainable Development

The procedure was further evaluated in terms of sustainability and health risks using three environmental assessment BAGI and ComplexGAPI metrics tools. The suitability of new solvents for extraction of pollutants and their analytical monitoring was examined with the BAGI software (Manousi et al. 2023). This software considers 10 factors that affect the overall assessment, including the number of analytes, chemical type, solvents, and required equipment (Section SM4, Table SM2). Figure 10 presents the pictogram generated after the BAGI evaluation of the proposed HDES-based extraction method. According to BAGI, a score of at least 60 points is needed for an approach to be deemed "acceptable." In this study, the green solvent extraction method achieved a BAGI score of 70.0, indicating good applicability, although certain aspects, such as automation, could still be optimized.

The sustainability of the developed method was assessed using the ComplexMoGAPI tool (Section SM4, Table SM2). The sample preparation stage shows a high degree of greenness, as it requires no preservation or transport steps and relies on simple microextraction and clean-up procedures under normal storage conditions. The use of green solvents and micro-scale extraction significantly reduces solvent consumption. The amounts of reagents used were below 10 mL per sample, with low health and safety hazards (NFPA scores ≤ 1). The method exhibits low energy consumption (≤ 1.5 kWh per sample), minimal waste generation (< 1 mL), and includes waste recycling, while hermetic operation minimizes occupational exposure. From an analytical perspective, satisfactory extraction yields (70–89%) were achieved under mild conditions, with integrated quantification and product purity exceeding 98%. The procedure fulfills five to six green economy criteria, and despite an E-factor of 88, the overall environmental impact remains acceptable due to the microextraction scale and recyclability of reagents. Overall, the ComplexMoGAPI assessment confirms that the proposed approach represents a green and sustainable analytical method for the extraction of diclofenac from aqueous samples.

4 Conclusions

1. Five menthol-based hydrophobic deep eutectic solvents (HDES) were synthesized using levulinic, acetic, lactic, oleic acids, and linalool as hydrogen-bond donors. ^{1}H, ^{13}C NMR and FTIR confirmed hydrogen-bonded networks between menthol and each donor. Frontier molecular orbital calculations revealed varying reactivities: levulinic acid was the strongest electrophile ($\omega = 2.42$ eV), while linalool was the softest and most reactive ($\Delta E = 10.43$ eV). MEP analysis showed the amphiphilic nature of menthol and complementary donor/acceptor sites of the acids and linalool. Levulinic, acetic, and lactic acids had intermediate polarity ($\Delta V = 0.701$–0.798 a.u.), oleic acid the largest

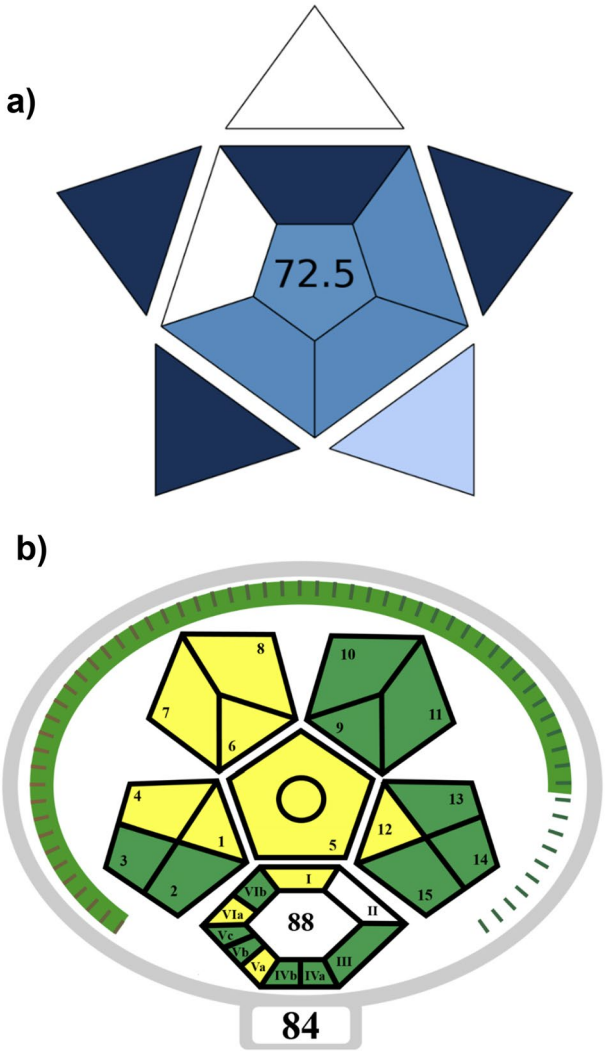

Fig. 10 Pictograms of blue applicability grade index (BAGI) (**a**) and ComplexGAPI (**b**)

(1.275 a.u.), and linalool the smallest (0.552 a.u.), reflecting their hydrogen-bonding capabilities within HDES.

2. Menthol-based HDESs exhibited low polarity that can be effectively tuned by the choice of hydrogen-bond donor. Nile red measurements showed E_TN values from 52.46 to 57.18 kcal·mol^{-1}, confirming that donor selection controls the solvent microenvironment, making these HDESs promising for bioactive and extraction applications.
3. Comparative analysis of menthol-based deep eutectic solvents showed that antibacterial activity depends on the hydrogen-bond donor. Menthol–linalool exhibited the highest effect via synergistic membrane disruption, menthol–acetic acid showed moderate activity through membrane permeabilization and acidification, and menthol–oleic acid was least effective due to high hydrophobicity and weak acidity.

4. Menthol-based HDESs efficiently extracted methylene blue (65–84%) and diclofenac sodium (≈55%), with extraction efficiency depending on solvent polarity and clear phase separation, confirming effective dye removal. The extraction efficiency of the studied HDES is strongly dependent on their solvatochromic parameters. Dye removal is favored in more hydrophobic systems with low α and β values, where hydrophobic interactions dominate. In contrast, diclofenac extraction is governed by dipolarity (π*) and hydrogen-bond donor ability (α), requiring more polar systems capable of specific interactions. Overall, the results confirm that extraction efficiency is compound-dependent and can be effectively tuned by adjusting the solvatochromic properties of HDES. Menthol-based HDES combine selective extraction of polar or nonpolar pollutants with intrinsic antimicrobial activity, making them promising multifunctional and sustainable solvents for integrated water treatment.
5. The developed HDES-based vortex-assisted microextraction method provides efficient extraction of diclofenac from aqueous samples, achieving yields of 70–89% under mild conditions with low solvent and energy consumption. Sustainability assessments using ComplexGAPI, and ComplexMoGAPI confirm strong compliance with the principles of Green Analytical Chemistry, highlighting the method as an environmentally friendly alternative for pharmaceutical contaminant analysis.

Supplementary Information The online version contains supplementary material available at https://doi.org/10.1007/s40710-026-00832-3.

Author Contributions Victoria Vorobyova: Conceptualization, Methodology, Investigation, Writing – review and editing. Georgii Vasyliev: Formal analysis, Writing – review and editing. Oleksiy Myronyuk: Investigation, Visualization. Inna Trus: Visualization. Margarita Skiba: Conceptualization, Methodology, Investigation, Visualization, Writing – review and editing.

Funding This work was carried out within the framework of the NRFU grant "Advanced Science in Ukraine 2026–2028" [grant No. 2025.07/0078].

Data Availability No datasets were generated or analysed during the current study.

Declarations

Competing interests The authors declare no competing interests.

References

Abranches DO, Coutinho JAP (2022) Type V deep eutectic solvents: design and applications. Curr Opin Green Sustain Chem 35:100612. https://doi.org/10.1016/j.cogsc.2022.100612

An Y, Row KH (2021) Evaluation of menthol-based hydrophobic deep eutectic solvents for the extraction of bisphenol A from environment water. Anal Lett 54:1533–1545. https://doi.org/10.1080/00032719.2020.1811716

Arcon DP, Franco FC, Jr (2020) All-fatty acid hydrophobic deep eutectic solvents towards a simple and efficient microextraction method of toxic industrial dyes. Journal of Molecular Liquids 318(15): 114220 https://doi.org/10.1016/j.molliq.2020.114220

Azmi NAN, Elgharbawy AAM, Mohd Salleh H, Hayyan A (2021) Evaluation of the antimicrobial performance of menthol and menthol-based deep eutectic solvents as potential future antibiotic. E3S Web Conf 287:02010. https://doi.org/10.1051/e3sconf/202128702010

Bagović Kolić M, Železnjak M, Markov K, Gaurina Srček V, Cvjetko Bubalo M, Radošević K, Radojčić Redovniković I (2025) Physicochemical and biological properties of menthol and thymol-based natural deep eutectic solvents. Molecules 30:1713. https://doi.org/10.3390/molecules30081713

Berry JD, Neeson MJ, Dagastine RR, Chan DYC, Tabor RF (2015) Measurement of surface and interfacial tension using pendant drop tensiometry. J Colloid Interface Sci 454:226–237. https://doi.org/10.1016/j.jcis.2015.05.012

Bochko T, Andrusenko E, Glushakov R et al (2025) Hydrophilic deep eutectic solvents for bioactive compound extraction from *Rubia tinctorum* L. Anal Bioanal Chem 417:4251–4263. https://doi.org/10.1007/s00216-025-05941-w

Cao J, Su E (2021) Hydrophobic deep eutectic solvents: the new generation of green solvents for diversified and colorful applications in green chemistry. J Clean Prod 314:127965. https://doi.org/10.1016/j.jclepro.2021.127965

Castro VI, Craveiro R, Silva JM, Reis RL, Duarte ARC (2023) Antimicrobial potential of natural deep eutectic solvents. Lett Appl Microbiol 75:607–617. https://doi.org/10.1093/lambio/lad029

Chen E, Zhang Y, Wang Y et al (2025) Research status and future trends of deep eutectic solvents in the field of natural medicinal chemistry. J Therm Anal Calorim. https://doi.org/10.1007/s10973-025-14871-9

Cysewski P, Jeliński T, Kukwa O, Przybyłek M (2025) From molecular interactions to solubility in deep eutectic solvents: Exploring flufenamic acid in choline-chloride- and menthol-based systems. Molecules 30:3434. https://doi.org/10.3390/molecules30163434

Duque A, Sanjuan A, Bou-Ali MM, Alonso RM, Campanero MA (2023) Physicochemical characterization of hydrophobic type III and type V deep eutectic solvents based on carboxylic acids. J Mol Liq 392:123431. https://doi.org/10.1016/j.molliq.2023.123431

Falahudin A, Insin N, Khan MM, Synthesis (2025) Properties, applications, and future directions. J Chem Eng Data 70:4880–4900. https://doi.org/10.1021/acs.jced.5c00578

Farias GC, Giaretta L, de Souza AM, da Silva DT (2025) Physicochemical and biological properties of menthol- and thymol-based natural deep eutectic solvents. Int J Mol Sci 26:10218. https://pubmed.ncbi.nlm.nih.gov/40333624/

Ferreira KC, Isquibola G, de Souza LM, Ribeiro CA, Caires FJ, Gonzalez MH, de Gomes PCF L (2026) Characterization of hydrophobic deep eutectic solvents to evaluate their application as a solvent in dispersive liquid–liquid microextraction in liquid environmental samples. J Mol Liq 446:129322. https://doi.org/10.1016/j.molliq.2026.129322

Guidugli LF, Reza T (2025) Systematic evaluation of stearic acid-based hydrophobic deep eutectic solvents on the extraction of selected light and heavy rare earth elements from water. J Ionic Liq 5:100176. https://doi.org/10.1016/j.jil.2025.100176

Huang et al (2021) Opendrop: open-source software for pendant drop tensiometry and contact angle measurements. J Open Source Softw 6:2604. https://doi.org/10.21105/joss.02604

Ivanova D, Apostolov A, Tuleshkov P, Novakov C, Yankov D (2025) New menthol-based hydrophobic deep eutectic solvents as a tool for lactic acid extraction. Appl Sci Basel 15:3564. https://doi.org/10.3390/app15073564

Jabbarvand BN, Jahanbin S (2025) The effect of an external electric field (EEF) on deep eutectic solvent based on monoterpenes (V type DESs) with molecular dynamics simulation approach. J Eng Rep 7:70290. https://doi.org/10.1002/eng2.70290

Kumar G, Kumar K, Bharti A (2024) Quantum chemistry-based approach for density prediction of non-ionic hydrophobic eutectic solvents. J Solut Chem 53:1195–1210. https://doi.org/10.1007/s10953-024-01372-w

Langhals H (2023) How the concept of solvent polarity investigated with solvatochromic probes helps studying intermolecular interactions. Liquids Basel 3:481–511. https://doi.org/10.3390/liquids3040031

Li B, Shi M, Qin S et al (2025) Antibacterial mechanism of hydrophobic deep eutectic solvents-in-water nanoemulsion: experimental and molecular dynamic simulation studies. Food Measure 19:3429–3443. https://doi.org/10.1007/s11694-025-03192-y

Liu Y, Wang H, Xu Y, Wang D, Zhu X, Wang M, Teng J (2025) Menthol-based hydrophobic deep eutectic solvents for the purification of tea peroxidase using a three-phase partition method. LWT 218:117528. https://doi.org/10.1016/j.lwt.2025.117528

López-Flores FJ, Ramírez-Márquez C, González-Campos JB, Ponce-Ortega JM (2025) Machine learning for predicting and optimizing physicochemical properties of deep eutectic solvents: review and perspectives. Ind Eng Chem Res 64:3103–3117. https://doi.org/10.1021/acs.iecr.4c03610

Malik A, Dhattarwal HS, Kashyap HK (2022) An overview of structure and dynamics associated with hydrophobic deep eutectic solvents and their applications in extraction processes. ChemPhysChem 23:e202200239. https://doi.org/10.1002/cphc.202200239

Mannu A, Di Pietro ME, Carotti C, Magugliani G, Mossini E, Macerata E, Rozas S, Aparicio S, Mele A (2025) Low melting mixtures from waste as leaching agents for black mass processing. J Mol Liq 435:128161. https://doi.org/10.1016/j.molliq.2025.128161

Manousi N, Wojnowski W, Płotka-Wasylka J, Samanidou V (2023) Blue applicability grade index (BAGI) and software: a new tool for the evaluation of method practicality. Green Chem 25:7598–7604. https://doi.org/10.1039/d3gc02347h

Marchel M, Rayaroth MP, Wang C, Kong L, Khan JA, Boczkaj G (2023) Hydrophobic (deep) eutectic solvents (HDESs) as extractants for removal of pollutants from water and wastewater – a review. Chem Eng J 475:144971. https://doi.org/10.1016/j.cej.2023.144971

Nakhle L, Kfoury M, Mallard I, Greige-Gerges H, Landy D (2022) Solubilization of *Eucalyptus citriodora* essential oil and citronellal in deep eutectic solvents:water:cyclodextrins mixtures. J Mol Liq 359:119371. https://doi.org/10.1016/j.molliq.2022.119371

Ojeda GA, Vallejos MM, Samorì C, Galletti P (2025) Hydrophobic eutectic solvents for sustainable recovery of carotenoids from mango peel: extraction optimization and insights into molecular interactions at play. J Mol Liq 425:127264. https://doi.org/10.1016/j.molliq.2025.127264

Pachernegg L, Maier J, Yagmur R, Damm M, Kalb R, Coclite AM, Spirk S (2024) Physicochemical properties of 20 ionic liquids prepared by the carbonate-based IL (CBILS) process. J Chem Eng Data 69:1814–1823. https://doi.org/10.1021/acs.jced.3c00687

Pishro KA, Silva LS, Lamarca RS, Amaral CDB, Gonzalez MH (2025) Exploring caffeine extraction using hydrophobic deep eutectic solvents: experimental and theoretical approaches. ACS Omega 10:44218–44233. https://doi.org/10.1021/acsomega.5c05673

Plyduang T, Wangpradit N, Phanapithakkun S, Nuntawong P, Sakamoto S, Suksamrarn A, Yusakul G (2025) Hydrophobic deep eutectic solvents and their microemulsion systems for solubility and microwave-assisted extraction of (3R)-1,7-diphenyl-(4E,6E)-4,6-heptadien-3-ol from *Curcuma comosa* Roxb. Microchem J 212:113200. https://doi.org/10.1016/j.microc.2025.113200

Quaid T, Reza T (2023) COSMO-RS predictive screening of type 5 hydrophobic deep eutectic solvents for selective platform chemicals absorption. J Mol Liq 382:121918. https://doi.org/10.1016/j.molliq.2023.121918

Ribeiro BD, Florindo C, Iff LC, Coelho MAZ, Marrucho IM (2015) Menthol-based eutectic mixtures: hydrophobic low viscosity solvents. ACS Sustain Chem Eng 3:2469–2477. https://doi.org/10.1021/acssuschemeng.5b00532

Riyana H, Harlia, Rahmalia W (2025) Highly efficient extraction of cationic dye (methylene blue) from aqueous solution using thymol-lauric acid-based deep eutectic solvents. J Mol Liq 439:128818. https://doi.org/10.1016/j.molliq.2025.128818

Rodríguez-Juan E, López S, Abia R, Muriana FJG, Fernández-Bolaños J, García-Borrego A (2021) Antimicrobial activity on phytopathogenic bacteria and yeast, cytotoxicity and solubilizing capacity of deep eutectic solvents. J Mol Liq 337:116343. https://doi.org/10.1016/j.molliq.2021.116343

Sanches MA, Farias GC, Giaretta L, Ferreira ML (2023) Menthol-based deep eutectic systems as antimicrobial and anti-inflammatory agents for wound healing. J Mol Liq 372:121205. https://doi.org/10.1016/j.molliq.2022.121205

Shah PA, Chavda V, Hirpara D et al (2023) Exploring the potential of deep eutectic solvents in pharmaceuticals: challenges and opportunities. J Mol Liq 390:123171. https://doi.org/10.1016/j.molliq.2023.123171

Shah M, Singh PS, Priyanka N, Devi TG (2025) Synthesis and characterization of hydrophobic and hydrophilic deep eutectic solvents: spectroscopic, DFT, molecular docking analysis. J Mol Liq 429:127584. https://doi.org/10.1016/j.molliq.2025.127584

Shahzad S, Arain MB, Soylak M (2026) Switchable deep eutectic solvents: types, sample preparation strategies, and applications in food and environmental analysis. Microchem J 224:117450. https://doi.org/10.1016/j.microc.2026.117450

Shakourian-Fard M, Ghenaatian HR, Alizadeh V, Kamath G, Khalili B (2021) Density functional theory investigation into the interaction of deep eutectic solvents with amino acids. J Mol Liq 343:117624. https://doi.org/10.1016/j.molliq.2021.117624

Siddiqui M, Ali M (2026) Sustainable extraction of hydrophobic azo dyes using recyclable fatty acid–based deep eutectic solvents for industrial wastewater remediation. ACS EST Water 6:756–772. https://doi.org/10.1021/acsestwater.5c00871

Silva JM, Silva E, Reis RL, Duarte ARC (2019) A closer look in the antimicrobial properties of deep eutectic solvents based on fatty acids. Sustain Chem Pharm 14:100192. https://doi.org/10.1016/j.scp.2019.100192

Singh MB, Prajapat A, Jain P et al (2024) Investigate the significance of DES to enhance the solubility of noscapine: DFT calculations, MD simulations, and experimental approach. Ionics 30:1795–1813. https://doi.org/10.1007/s11581-023-05359-3

Sportiello L, Favati F, Condelli N, Di Cairano M, Caruso MC, Simonato B, Tolve R, Galgano F (2023) Hydrophobic deep eutectic solvents in the food sector: focus on their use for the extraction of bioactive compounds. Food Chem 405:134703. https://doi.org/10.1016/j.foodchem.2022.134703

Thiamngoen P, Pinpatthanapong K, Juntadech NC et al (2024) Preparation of cellulose fiber from cattail using two-stage pretreatment and choline chloride-oxalic acid deep eutectic solvent extraction for oil adsorption. Environ Process 11:35. https://doi.org/10.1007/s40710-024-00702-w

Viñas-Ospino A, Panić M, Bagović M, Radošević K, Esteve MJ, Radojčić Redovniković I (2023a) Green approach to extract bioactive compounds from orange peel employing hydrophilic and hydrophobic deep eutectic solvents. Sustain Chem Pharm 31:100942. https://doi.org/10.1016/j.scp.2022.100942

Viñas-Ospino A, Panić M, Radojčić-Redovniković I, Blesa J, Esteve MJ (2023b) Using novel hydrophobic deep eutectic solvents to improve a sustainable carotenoid extraction from orange peels. Food Biosci 53:102570. https://doi.org/10.1016/j.fbio.2023.102570

Vorobyova VI (2023) Plant extract based on deep eutectic solvent-mediated biosynthesis of silver nanoparticles: Cytotoxicity and antibacterial effects. Bioinorg Chem Appl 2023:9672432. https://doi.org/10.1155/2023/9672432

Vorobyova VI, Linyucheva OV, Chygyrynets OE, Skiba MI, Vasyliev GS (2022) Comprehensive physicochemical evaluation of deep eutectic solvents: Quantum-chemical calculations and electrochemical stability. Mol Cryst Liq Cryst 750:60–68. https://doi.org/10.1080/15421406.2022.2073037

Vorobyova V, Vasyliev G, Skiba M et al (2023) Green extraction of phenolic compounds from grape pomace by deep eutectic solvent extraction: Physicochemical properties, antioxidant capacity. Chem Pap 77:2447–2458. https://doi.org/10.1007/s11696-022-02635-w

Vorobyova V, Skiba M, Vasyliev G (2024) Deep eutectic solvents: Quantum chemical investigation, thermal stability and physicochemical properties. Chem Phys 586:112401. https://doi.org/10.1016/j.chemphys.2024.112401

Zeng C, Liu Y, Ding Z, Xia H, Guo S (2021) Physicochemical properties and antibacterial activity of hydrophobic deep eutectic solvent-in-water nanoemulsion. J Mol Liq 338:116950. https://doi.org/10.1016/j.molliq.2021.116950

Zheng GK, Rozi SKM, Ang QY et al (2025a) Hydrophobic deep eutectic solvent with antibacterial activity for remediation of crystal violet dye: Experimental and theoretical investigations. Int J Environ Sci Technol 22:13731–13747. https://doi.org/10.1007/s13762-025-06529-8

Zheng X, Yin F, Gong G, Zhang X, He S, Tang W, Wei X-H (2025b) An overview of hydrophobic deep eutectic solvents driven liquid-phase extraction: Applications and prospects. J Chromatogr A 1748:465824. https://doi.org/10.1016/j.chroma.2025.465824

Authors and Affiliations

Victoria Vorobyova[1] · Georgii Vasyliev[1] · Oleksiy Myronyuk[1] · Inna Trus[1] · Margarita Skiba[2]

✉ Victoria Vorobyova
vorobyovavika1988@gmail.com

Georgii Vasyliev
g.vasyliev@kpi.ua

Oleksiy Myronyuk
airshape@ukr.net

Inna Trus
inna.trus.m@gmail.com

Margarita Skiba
margaritaskiba88@gmail.com

[1] Chemical Technology Department, National Technical University of Ukraine ″Igor Sikorsky Kyiv Polytechnic Institute″, Kyiv 03056, Ukraine

[2] Department of Inorganic Materials Technology and Ecology, Ukrainian State University of Science and Technologies, Dnipro 49005, Ukraine